Production of menthol-loaded polymeric nanoparticles by solvent displacement

Full text of the paper published on
Canad. J. Chem Eng. **95**(9), 1690-1706 (2017)
[DOI: 10.1002/cjce.22867].

Available at: **https://doi.org/10.1002/cjce.22867**
Supporting information: cjce22867-sup-0001-SuppInfo-S1.pdf

Production of menthol-loaded nanoparticles by solvent displacement

Ferri A.*, Kumari N., Peila R. and Barresi A. A.

Department of Applied Science and Technology, Politecnico di Torino

Corso Duca degli Abruzzi 24, 10129 Torino (Italy)

Abstract

The production of producing menthol-loaded poly-ε-caprolactone nanoparticles (NPs) for dermal application was investigated. The nanoparticles were produced in three different mixers: a confined impinging jet mixer (CIJM), a two-inlet vortex mixer (VM) and a four-inlet vortex mixer (MIVM), testing their performances in the same operating conditions. The effects of various process parameters such as polymer and menthol concentration, flow rate, solvent type (acetone, acetonitrile or THF) and quench ratio, on mean nanoparticle size, menthol loading and encapsulation efficiency were compared and discussed. The amount of menthol encapsulated inside the nanoparticles was quantified by GC analysis and the structure and shape of the NPs were analyzed by TEM.

Nanoparticles of size between 200 nm to 800 nm were obtained using the CIJM, the VM and the MIVM with different feeding sequence. It was observed that mixer geometry had a strong effect on particle size (at the same operating conditions the size decreased from MIVM with two inlets to VM and to CIJM) and the smallest particles were obtained using the MIVM using one solvent and three antisolvent streams. By using acetonitrile, the mean nanoparticle size was larger. Incorporation efficiency and menthol loading values up to 80% and 60% respectively were obtained depending on the inlet menthol and polymer concentrations.

Keywords: Solvent displacement, Confined-Impinging-Jet mixer, Vortex mixer, PCL, menthol.

* Corresponding author.

INTRODUCTION

In cosmetics and pharmaceutics, many active principles are encapsulated in polymers shells or dispersed in polymer matrices because of the benefits of encapsulation, which are mainly: (1) protection of the active principle in adverse environments; (2) controlled release of the active principle or (3) precision targeting. The typical size of nanoparticles ranges from 10 nm to 1000 nm depending on specific application and production method.[1-5]

Besides cosmetics and pharmaceuticals, microencapsulation is also of interests for the textile field where developments of medical and technical textiles have encouraged the industry to use microencapsulation as a mean of imparting textiles durable finishes with several purposes, such as anti-odor, antimicrobial and controlled release of active principles.[6]

In fact, a variety of bioactive molecules can be delivered through human skin, which not only works as a permeation barrier (mainly due to the stratum corneum layer), but also provides a unique delivery pathway for therapeutic and other active agents.[7] These compounds penetrate via intercellular, intracellular and trans-appendageal routes, resulting in topical delivery (into skin strata) or transdermal delivery (to subcutaneous tissues and into systemic circulation). Considering dermal and transdermal applications, the typical NP size generally varies and depends on the materials involved for NP production; however, a size cut off of 500 nm would seems appropriate but it is still an issue of debate and further investigation is needed.[8, 9]

As an example of drugs for topical delivery, menthol has a long tradition, as it is frequently part of topical antipruritic, antiseptic, analgesic and cooling formulations.[10, 11] Menthol has been used as refreshing agent for centuries and its mechanism of action is based on the activation of the same thermal receptor as cool temperature (between 8 to 28°C).[12-14] Menthol also belongs to the family of penetration enhancers, namely it increases the accessibility of other drugs through skin.[15] This effect may be explained by menthol's ability to disrupt the lipid bilayer of the stratum corneum, as well as forming pools within it.[16, 17]

Polymers are increasingly preferred to produce nanoparticles able to deliver drugs to the tissues or cells of interest.[18-20] The effectiveness of these systems strongly depends on the structure of the vehicle and, in particular, on the mean size and particle size distribution. Polymers are selected for preparing nanoparticles due to their versatility and fine tuning of their physico-chemical properties, which can possibly be altered to obtain the desired nanoparticle size. Natural polymers (*e.g.* chitosan), synthetic biodegradable polymers (*e.g.* poly-lactide-*co*-glycolide and poly-ε-caprolactone) as well as non-degradable polymers (*e.g.* polyacrylates) are the most widely used polymers in nanoparticle formation.

Polymeric nanoparticles can be subdivided in nanospheres and nanocapsules;[19-21] nanospheres have a monolithic-type structure (matrix) in which drugs are dispersed or absorbed on the surfaces or in the particles, but it is also possible to end-functionalize the polymer (an example with PCL end-functionalized with cumarin moieties is reported in [22]). Nanocapsules are vesicular system with an inner solid or liquid core surrounded by a polymeric membrane. In this case the active substance is usually dissolved in the inner core (or constitutes the solid core), but may also be adsorbed onto the capsule surface.

In certain cases, the distinction between nanospheres and nanocapsules is sharp and clear: for instance, when capsules with a liquid core are formed using oils, or low molecular weigth anphiphilic block copolymers are employed to encapsulate a solid hydrophobic active principle. When a preformed high molecular weight polymer, such as PCL, and an active principle which can oil out, such as menthol in the present work, are considered, uncertain, mixed or hybryd structures can be obtained; thus, in the following, we will generically call 'nanoparticles' the product of the nanoprecipitation process.

Polymer micelles also deserve mention, as they are attracting growing interest due to their small size; they consist of amphiphilic macromolecules with distinct hydrophobic and hydrophilic domains, which reversibly assemble in contact with water. The amphiphilic core/shell structure also favours entrapping of hydrophobic drugs, but the synthesis of amphiphilic block copolymers is quite complex and expensive.[23-26] Amphiphilic block copolymers are also often employed as surfactants to stabilize polymer nanoparticles or the precipitated API core.

Different methods can be applied to synthesize polymer nanoparticles, each one having its own advantages and limitations.[21, 27, 28] Emulsification-solvent evaporation was one of the first methods to obtain nanoparticles (even if it can hardly generate nanoparticles below 200 nm in diameter); high-speed homogenization or ultrasonication is employed to obtain controlled uniform particle size.[29] The emulsification-diffusion technique does not require homogenization and leads to good encapsulation efficiencies, but large volumes of water must be removed, with possible significant leakage of water-soluble active substances.[30]

The solvent-displacement technique (also known as flash precipitation) is based on dissolving the active principle and the polymer in a solvent and mixing the solution with an antisolvent (usually water), in which they are immiscible. This method allows to use solvents with low toxic potential, and also to encapsulate hydrophobic compounds within nanoparticles of water soluble polymers.[31, 32] Surfactants are often added in the synthesis, but it has been shown that they act only as stabilizing agents, and are not directly involved in the nanoparticles

formation process, while stable nanoparticles can be obtained even without surfactants if they have a surface charge, for examples as a consequence of the use of an initiator. [33, 34] The influence on nanoparticle size is generally weak and sometimes negative (smaller particles can be obtained without surfactant addition) and only long term stability is affected. Obviously in case of charged surfactants the ionic strength can affect the assembling process.

The size of the NPs depends significantly on the rate, magnitude and uniformity of super-saturation generated during NPs preparation. Special micromixers can be designed to achieve effective mixing, improving reproducibility and controlling particle size distribution; in fact, high super-saturation can be developed by intensive mixers in less time than required for nucleation and growth of precipitating solutes, and thus super-saturation brings the spontaneous formation of nanoparticles in the nano size limits.[26, 35-38]

Since nanoparticle formation is very fast, this process is mixing sensitive, or in other words it depends on the way solvent and anti-solvent are mixed. It is very well known that the size of the nanoparticles is greatly affected by the operating conditions, inlet feed composition and flow rate, but also by mixer type and geometry.

T-mixer has been commonly applied for fast chemical reactions; its design has been improved by adding a mixing chamber leading to the confined impinging jets mixer (CIJM) to enhance product yield and conversion efficiency[39]. Besides the production of polymer nanoparticles by flash precipitation.[38, 40-43], CIJM is used today in many biological, biochemical and chemical applications. Rapid mixing in CIJM is due to its geometry, which produces a region of high turbulent energy dissipation where the streams are forced to flow through, avoiding bypassing.[44-46] Johnson and Prud'homme[39] showed that internal hydrodynamics can be significantly affected by geometrical parameters, particularly the ratio of inlet tube-to-chamber diameter, the height and bottom shape of the mixing chamber, which in turn affects the final particle size. Scale up of geometrically similar mixing devices is possibile using the jet Reynolds number defined as $Re_j = \rho V_j d_{in}/\mu$.[45, 47, 48]

As a major disadvantage of CIJM, the best mixing performance is obtained employing two streams with the same flow rate (thus identical momentum), but this could limit the super-saturation level achievable inside the CIJM mixer.[44, 48, 49] To overcome this problem Liu and coworkers[50] developed the multi inlet vortex mixers (MIVM), which uphold the performance of the CIJM allowing higher flexibility in feeding flow rates and composition, including the possibility to feed drug and polymer in different streams. Moreover, as immediate sufficient dilution is achieved directly inside the chamber in MIVM,[51-54] Ostwald

ripening caused by the relatively high concentration of dissolved polymer in the outlet stream of CIJM can be avoided.

Finally, the literature evidenced that the solvent can significantly affect final particle size; in laminar conditions, this has been ascribed to viscosity, surface tension (Marangoni effect) and diffusivity. The greatest the solvent diffusion coefficient in water and the smallest the nanoparticles formed, confirming that diffusion rate plays a role in nanoprecipitation; this effect was clearly visible when homologous series of solvents, for instance alcohols, were used as solvents.[55] Solvent highly influenced particle size also in case of turbulent mixing, as it happens in intensive micromixers, even if viscosity does not play a role in this condition. Nevertheless, it is well known that solvent characteristics and differences in polymer-solvent molecular interactions can influence diffusion and aggregation processes [37, 421, 56], even though no certain and quantitative explanation of this has been provided up to now.

The scope of this work was the investigation of operating parameters on the NPs formation process with the aim of tuning the size of PCL loaded nanoparticles to accomplish the requirement of different applications. Poly-ε-caprolactone is a synthetic polymer widely employed in nanoparticle formulations due to its biocompatibility, biodegradability and mechanical properties; it is permeable to low molecular weight drugs and can therefore be used for diffusion controlled delivery.[33, 57, 58] Moreover, due to its semi-crystalline structure, on the one hand PCL degradation is delayed compared with amorphous polyesters but, on the other hand, the presence of the amorphous fraction favours drug entrapment.[59]

Different encapsulants have been already reported in literature,[20, 37] including trygligerides (Miglyol) to form nanocapsules. Between the others, menthol, caffeine and melatonine (which significantly differ for solubility and hydrophobicity, as measured by the octanol-water partition coefficient), were proposed for textile applications and investigated in our previous works;[60, 61] it was noted that they affected only sligthly the final size of the particles and its dependence on mixing conditions.

Menthol encapsulation in PCL has been investigated in this paper, obtaining particles size in a relatively wide range (between 200 nm to 800 nm), depending on the operating conditions; this is an interesting result, as particle size also affects adhesion to fibres, and prelimary results evidenced that too small nanoparticles may be less efficient. Looking for a cost effective solution, use of expensive surfactants has been avoided; in fact, literature results have shown that PCL nanoparticles can be stable up to 20 days even in absence of surfactants,[33] . Moreover, once immobilized on the fabric we expect that NPs are not much affected by aggregation in the dry state.

In a previous work[62] menthol-PCL micro and nano-particles were dispersed on a fabric with the aim of providing a refreshing effect to compressive socks, widely used by patients affected by chronic venous insufficiency. Nano-sized or micro-sized particles were obtained by playing with initial PCL and menthol concentrations at the same MR; however micro-sized formulations, resulting from highly concentrated solutions, often showed non-monomodal size distributions. Good adhesion of PCL-microparticles to the fabric and no alteration of skin physiology was shown in that preliminary work, which proved the feasibility of the concept but did not investigate deeply the influence of relevant operating parameters; menthol loading and encapsulation efficiency, two fundamental data for determining fabric functionalization durability and process yield, were not quantified.

In this work, PCL nanoparticles with and without loaded menthol were produced by the solvent displacement method employing three different solvents and using three different intensive mixers: a confined impinging jet mixer (CIJM) and a multi inlet vortex mixer with two (VM) or four (MIVM) inlet streams. Size, morphology and quantification of menthol have been investigated and discussed in detail.

The research was carried out with the following goals:

1. Investigating the effect of solvent type on nanoparticle size produced by solvent displacement technique; acetone and acetonitrile were investigated, but some tests were carried out also using tetrahydrofuran for comparison purposes.
2. Investigating the effect of quench ratio on particle size; as no surfactant was employed, this process step becomes crucial to assure stability and size control;
3. Comparing different mixer configurations (CIJM and vortex mixers) and identifying the effects of operating conditions for each mixer: initial PCL and menthol concentration, quench ratio, mass ratio and solvent type were varied in order to modulate the particle size.

4 Evaluating menthol loading in PCL nanoparticles for different processing conditions.

The experimental campaign has also produced a large data set for loaded nanoparticles, in different solvents, that will be useful for further model validation. Combined first-principle modelling, population balances and Molecular Dynamics (MD) approaches are very promising for understanting the different particle formation mechanisms and their different contribution varying the operating conditions. Up to now, they have been applied to PCL only nanoparticles produced by acetone solutions, but in the next future it will be possible to extend to a wider range of conditions.

MATERIALS AND METHODS

Chemicals

The racemic menthol mixture and the poly-ε-caprolactone (PCL) polymer with an average molecular weight of 14,000 Da were obtained from Sigma Aldrich. Acetone, acetonitrile Chromasolv (HPLC grade) and tetrahydrofuran (THF), whose physico-chemical data are shown in Table 1, were also purchased by Sigma–Aldrich. Milli-Q RG system by Millipore R (Billerica, MA, USA) was used to produce ultrapure water employed in all experiments.

Table 1. Physico-chemical data of organic solvents used for nanoparticle synthesis at 25ºC.

SOLVENT	$D_{solvent,water}$ m^2/s	$D_{water,\ solvent,}$ m^2/s	***Relative permittivity***	***Chemical formula***
Acetone	1.14×10^{-9} [63]	4.56×10^{-9} [63]	21.0	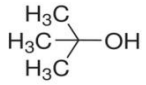
Acetonitrile	1.41×10^{-9} [63]	~$3.5\text{-}4 \times 10^{-9}$ [64]	37.5	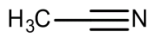
THF	5.0×10^{-10} [65]	8.0×10^{-10} [65]	7.5	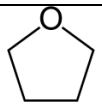

Menthol is highly soluble in many solvents but sparingly soluble in water (0.46 mg/mL at 25ºC).[10] This makes menthol a good candidate for the solvent displacement technique. The main physical properties of menthol are reported in Table S1 (Supplementray material).
Octanol-water partition of menthol confirms that menthol is hydrophobic, therefore it tends to stay in the lipophilic dermis and epidermis rather than reaching systemic circulation. Moreover, octanol-water partition coefficient of menthol suggests good affinity with PCL, which is hydrophobic as well.[66]

Synthesis of Menthol-PCL Nanoparticles

The proper amounts of PCL and menthol were weighted with accuracy of 0.001 g, dissolved in the selected solvent and maintained in a thermostatic bath at 40°C for half an hour to

guarantee complete solubilization.

No surfactant was added, as discussed in the introduction; preliminary esperiments using Poloxamer 388 evidenced no significant effect on the pure PCL particle size, while the zeta potential was strongly reduced.[67]

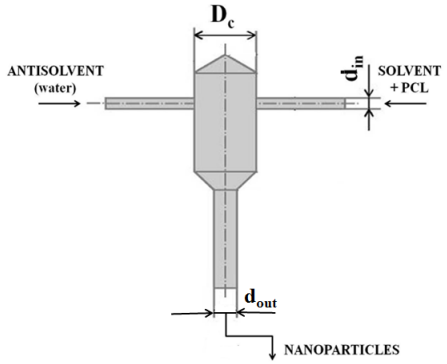

Figure 1. Sketch of the confined impinging jet mixer (CIJM) used for the preparation of nanoparticles. (d_{in} = 1 mm, d_{out} = 2 mm, D_c = 5 mm, total chamber height = 11.2 mm).

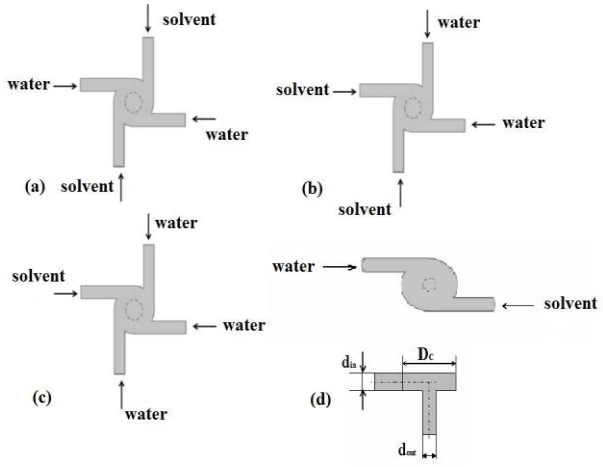

Figure 2. Tested feeding configurations for the vortex mixer with four and two feeding streams. d_{in}= 1 mm, d_{out}= 2 mm, D_c = 4 mm. PCL and menthol were always fed together in the solvent streams.

Solvent and antisolvent (water) were put in 100-mL syringes and placed in the syringe pumps (KDS200, KD Scientific, USA). The syringes were connected via plastic tubes of inner diameter 1 mm with the feed tubes of the CIJM or the vortex mixer (VM & MIVM). The schemes of the two mixers are illustrated in Figures 1 and 2. In case of the MIVM, different feeding configurations were investigated, changing the sequence of solvent and antisolvent (SWSW or SSWW, as shown in Figure 2a and 2b) or using a single solvent feed and three water streams (SWWW in Figure 2c). The same device was employed to investigate the

performances of the two-streams vortex mixer, using only two opposite feeding tubes (SW in Figure 2d).

The feed flow rate for each inlet was varied from 5 mL/min to 120 mL/min, corresponding to inlet jet velocity from about 0.1 to 2.5 m/s, and the flow rates of solvent and antisolvent were always kept equal; in the MIVM the solvent stream composition was the same for all streams, containing both polymer and menthol.

The outlet stream was quickly diluted in ultrapure water and gently stirred to stabilize the nanoparticle suspension. Dilution, called quench, avoids size increase by Ostwald ripening, which can be significant as the solvent concentration was reduced only by 50% v/v by mixing with anti-solvent. Further dilution was not required in case of MIVM with SWWW configuration, where three water streams assured quench already inside the mixer. Different quench ratios *QR*, namely the ratio of anti-solvent to quench water volume, were investigated (from 0.12 to 1), to find optimal conditions in case of menthol-loaded nanoparticles. Previous results evidenced that quench is essential, to avoid large particle size increase, especially for loaded nanoparticles. However, data obtained with PCL only particles evidenced that large dilution volumes, in practice $QR<0.5$, are not convenient since negligible further size reduction can be obtained by increasing dilution. For *QR* values between 0.5 to 1, some size increase was observed but this effect was acceptable if compared with the convenience of less water to remove from the formulation.[37, 49]

Table 2. Operating conditions in the CIJM and vortex mixers.

OPERATING PARAMETERS	**RANGE**
Inlet PCL concentration, C_{PCL}	3 – 15 mg/mL
Inlet menthol concentration	1.5 – 24 mg/mL
Menthol to polymer mass ratio in the feed (*MR*)	0.76 – 2
Single jet feed flow rate (Jet velocity, V_j)	5 – 120 mL/min (0.1 – 2.5 m/s)
Quench volumetric ratio (*QR*)	0.12 – 1

The operating conditions considered in this work are summarized in Table 2. The experiments were carried out at room temperature in a conditioned environment (25±1°C) but no control of flow streams temperature was implemented in the experimental set-up. For comparison purposes PCL nanoparticles without menthol were produced at the same process conditions.

Nanoparticle Characterization

The nanoparticles were characterized in terms of their size distribution and Zeta potential by using DLS Zetasizer Nanoseries ZS90, Malvern Instrument, UK. Mean size value from the intensity distribution, *Z* average, and polydispersity index, PdI, a dimensionless measure of the broadness of the size distribution calculated from the cumulants analysis, have been reported. A few examples of the reconstituted particle size distribution (PSD) have been also shown. Samples were prepared diluting 0.1 mL of NPs suspension in 1 mL of ultrapure water. Measurements were carried out at 25.0±0.1°C in a thermostatized cell; analysis were done in triplicate and the average value was considered.

Nanoparticles were separated by centrifugation (Thermo scientific F15-6x100) for DSC analysis and loading evaluation. The centrifugation time and speed were investigated to limit nanoparticle damage and ensure the maximum NPs recovery: a clear supernatant was obtained in 35 minutes at 12,000 rpm (corresponding to 22,600 g).

DSC analyses of unloaded and menthol-loaded nanoparticles were carried out in a DSC model Q200 (TA Instruments, New Castle, DE, USA) using sealed aluminum pans in nitrogen flow. Samples were heated at 5°C/min and cycles were repeated after cooling and equilibration at 20°C; a few cycles were also carried out after stabilization at 40°C, to favor menthol melting and verify menthol encapsulation.

The morphology of the nanoparticles was investigated by means of JEOL JEM-2010F transmission electron microscopy (TEM) at an accelerating voltage of 80 kV.

The procedure for menthol quantification is summarized below:

(1) Nanoparticles recovery by centrifugation

(2) Menthol extraction by ethanol from the nanoparticles (extraction time: 1 h)

(3) Menthol quantification in the extract by Gas-cromatographic (GC) analysis

(4) PCL quantification by gravimetric analysis

(5) Loading capacity and incorporation efficiency estimation

As PCL is insoluble in ethanol,[68] after centrifugation, the solid NPs were rinsed in ethanol to remove interstitial liquor and dispersed in a known volume of ethanol at room temperature; complete extraction was obtained in 1 hour. Extraction time was set as the result of a series of experiments, with time varying from 20 to 150 minutes, considering both low and high *MR*: extracyed menthol increased almost linearly with time only up to 60 min, in all cases.

After centrifugation, menthol contained in the ethanol solution was analyzed by GC while solid PCL residue was dried at 30ºC overnight and weighted to quantify PCL gravimetrically. The GC analysis was performed by Hewlett-Packard, model 6890 gaschromatograph, equipped with a 30 m × 0.32 mm capillary column coated with a 0.25 μm film of cross-linked 5% phenyl methyl siloxane. Decanol was used as internal standard, as suggested in the literature.[69]

From the amount of extracted menthol and recovered PCL, incorporation efficiency and menthol loading were calculated. Loading capacity (LC) was defined in Equation (1) as the amount of active principle incorporated by the polymer expressed as weight percentage in the final formulation, whereas incorporation efficiency (IE) was defined in Equation (2) as the amount of active principle encapsulated by the polymer expressed as percentage of the total amount of drug fed to the mixer:

$$\mathbf{LC} = \frac{\textbf{Amount of incorporated menthol}}{\textbf{Total amount of nanoparticles}} \times 100 \qquad (1)$$

$$\mathbf{IE} = \frac{\textbf{Amount of incorporated menthol}}{\textbf{Total amount of menthol added in the process}} \times 100 \qquad (2)$$

RESULTS AND DISCUSSION

Nanoprecipitation in CIJM: Influence of Solvent Type and Operating Conditions

Previous results on nanoparticle formation by flash precipitation evidenced the dependence of particle size on internal hydrodynamics and mixing conditions, which can be related to inlet jet velocity, V_j, and on inlet polymer concentration. The choice of the proper solvent is of utmost relevance, as it influences strongly the final size of the particles, even if a priori prediction of the behavior of the polymer-solvent system is very difficult. Besides being highly nonlinear, the interaction between polymer molecules and solvent influences the initial steps of the formation process in a complex way, that only in a few cases has been at least partially understood. Molecular Dynamics simulations can supply useful information, but calculations are very complex and time-consuming, and have been carried out only for a limited number of cases.[37]

Thus, it is interesting to investigate experimentally the effect of different solvents in order to find optimal conditions for particle synthesis and to contribute to elucidate interaction mechanisms; in this work, the behaviour of acetone, acetonitrile and THF, three solvents with different chemical structure and physico-chemical characteristics were compared. As a first step, the influence of feed velocity and polymer concentration on PCL only particles with different solvent was investigated in the confined impinging jet mixer, in order to get reference data to compare with the results obtained for loaded particles. A quench ratio of 0.5 was used (that is the outlet collected suspension volume was diluted by an equal volume of quench water, which was double of that used as antisolvent in the mixer); results are shown in Figure 3.

The results confirm that the particle size decreased with increasing feed velocity and increased with increasing polymer concentration: the trend can be described in a relatively wide range, as suggested in previous works,[37] by a power-law equation, at least in the turbulent region for Re_j>310.[70]

$$d_p = A V_j^{\beta} C_{\mathrm{PCL}}^{\alpha} \tag{3}$$

The results obtained with acetone were in agreement with previous data obtained in the same mixer, with α = 0.29 and β= – 0.18.[49] The trend is similar for acetonitrile and THF; in particular the same dependence on hydrodynamics is observed, while the influence of the polymer concentration can change with the solvent considered, as previously reported for other polymers.[37] But particles are significantly larger than in acetone at the same operating

conditions (see a direct comparison in Figure S1, in the Supplementary material). This increase in particle size cannot be accounted for simply considering the different jet Reynolds number, because differences in viscosity between the water-solvent mixtures (that are in any case very small) are not relevant in turbulent conditions, even if they can affect diffusivity. For this reason, we preferred to plot data using the inlet jet velocity, that is the same for all solvents at the same flow rate. In fact, it was demonstrated that Re_j is useful only to scale up processes for the same polymer-solvent system and at the same inlet concentration, in mixer geometrically similar of different size.[48]

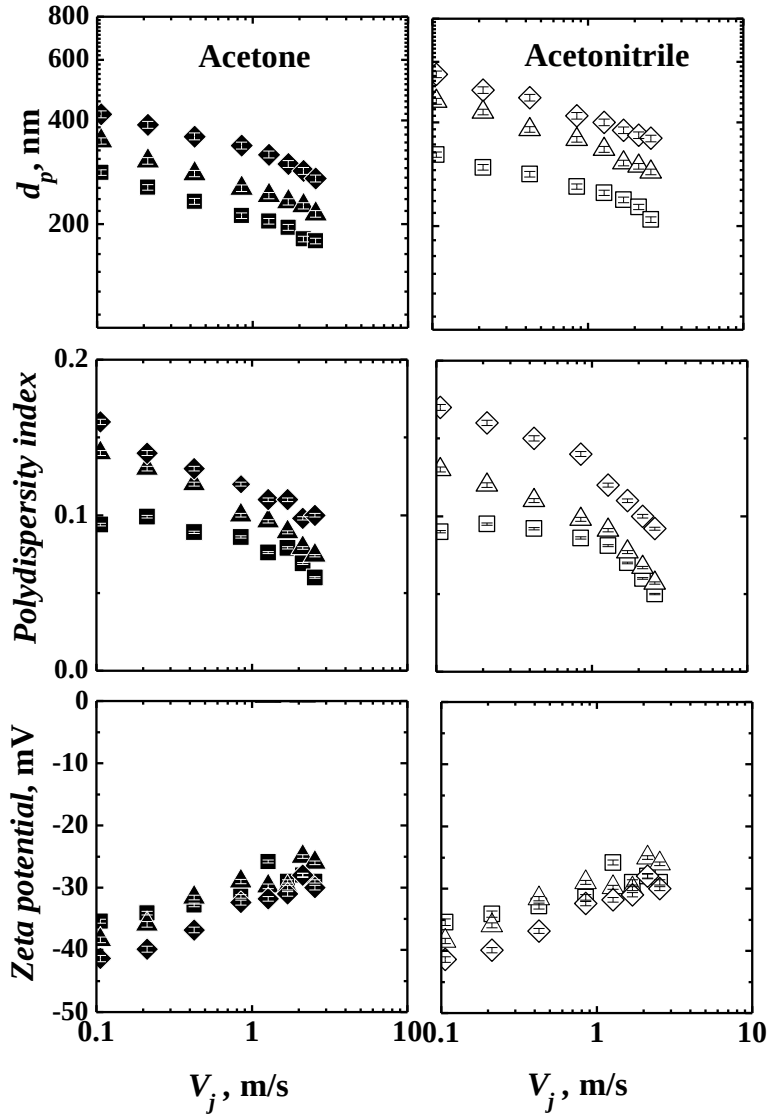

Figure 3. Influence of inlet feed velocity and polymer concentration on PCL only (unloaded) particles size, Polydispersity index (PdI) and zeta potential, using acetone (filled symbols) and acetonitrile (open symbols). Inlet polymer concentration, C_{PCL}: ■,□, 3 mg/mL; ▲,△, 6 mg/mL; ◆,◇, 9 mg/mL. *QR*=0.5. CIJM mixer.

Figure 3 also shows the variation of the polydispersity index and of the zeta potential. It can be observed that polydispersity index is alway small (lower than 0.2), which indicates a relatively narrow distribution. Moreover, it follows in general the trend of particle size (Z-average), decreasing further at higher feed velocity (and in case of acetonitrile the reduction is even stronger); this means not only that the particles became smaller by improving mixing but also that the distribution became narrower. Zeta potential values are always negative, and similar for acetone and acetonitrile (similar values were oberved also for THF). The nanoparticles are negatively charged due to the presence of ionized carboxylate end-groups of PCL polymeric chains on the particle surface;[71] it has been proposed that the weakly solvated ions interacts with the hydrophobic surfaces leading to a Zeta potential that reflect this anionic charging.[34] Values in the range –45 to –25 mV were observed, confirming that nanoparticles are stable even in absence of surfactants; it must be evidenced that in this case the mechanism of stabilization is electrostatic, while the presence of surfactants assure steric stabilization. Figure 3 also shows that the potential becomes less negative for particles obtained at higher jet velocity and lower inlet polymer concentration.

The particle formation process is complex and no general agreement exists in the literature. The role of mixer geometry and hydrodynamics in determining mixing conditions, local species concentration and supersaturation build up have been clarified with the help of Computational Fluid Dynamics (CFD),[44, 45, 50] but the effect of species concentration (and temperature) and the role of supersaturation itself is still a point of debate. Different mechanisms have been proposed to explain the observed dependence on operating conditions:referring to the classical nucleation theory, the nucleation-growth model or the nucleation-aggregation model have been proposed as limit cases, with possible intermediate conditions depending on the supersaturation level.

According to this approach, mixing of the two solvents creates a local supersaturation of the organic component, which leads to spontaneous (homogeneous) nucleation of solid particles; an energy activated process is supposed, whose rate should be strongly dependent on temperature and supersaturation. Growth can occur by deposition of single molecules onto the particle matrix after diffusion from the bulk, and depends on mass transfer coefficients and linearly on supersaturation. Actually, the classical nucleation theory was developed for inorganic substances, with assumptions that are hardly applicable to soft matter in flash nanoprecipitation; in particular, nucleation rate depends on the molecular volume of the organic component, which cannot be considered independent on the solvent-antisolvent

fraction in the liquid phase, which varies during the process.[35] To overcome these limitations, a modified nucleation model has been proposed, whose parameters in case of PCL precipitation from acetone-water mixtures were determined by Molecular Dynamics simulations.[72] MD simulations have shown that the dimension of a polymer molecule, or better the space occupied by it, estimated by the radius of giration, varies largely depending of the composition of the surrounding liquid phase.

Modeling work, based on population balance approach, has also evidenced that particle aggregation may take place in parallel to molecular growth. The aggregation rate depends on collision frequency of preformed particles, and thus is proportional to the second power of their number density (becoming relevant only at relatively high concentration), but depends weakly on temperature (considering that the aggregation kernel is proportional to absolute temperature and inversely proportional to fluid viscosity). Modeling evidenced also that Brownian aggregation is prevailing, while turbulent aggregation may contribute only when particles becomes larger than 200 nm.

Mixing, nucleation and molecular growth are in series, whereas aggregation occurs in parallel with growth; even though supersaturation is the driving force of all these processes, its influence is very different on nucleation and growth, respectively strong for the first and weak for the second one. The relative characteristic times determine the rate controlling process. As mixing (which causes the supersaturation build up) is influenced by hydrodynamics, it can be understood why preciptation is a mixing sensitive process: it must also be remembered that the slowest step controls the overall rate for processes arranged in series, while the fastest one determines the rate of parallel processes. Thus, large particles in case of poor mixing are explained with low nucleation rate, which finally leads to few big particles, considering that precipitation is almost complete in intensive mixers.

The explanation of the effect of species concentration is more complex. Unfortunately, local values of supersaturation, which are those really governing the process, are difficult to evaluate experimentally, and can be estimated only by means of CFD approach. Anyway, the expected influence of inlet concentration on final particle size, according to the different mechanisms, can be estimated. Assuming that supersaturation is directly related to inlet concentration, and that number of nuclei varies exponentially with supersaturation, in the nucleation-growth regime particle size should decrease with inlet polymer concentration. This behaviour has sometimes been observed, but it is much more common to observe an increase of particle size with initial polymer concentration described by a power-law relationship, compatible with a nucleation-aggregation mechanism.[73]

Alternatively to the mechanisms described above, based on an activated nucleation step, in some recent works the "ouzo effect" has been proposed to explain the initial spontaneous formation of nanoparticles by solvent displacement. When a hydrophobic solute is rapidly brought into the metastable region between the binodal and the spinodal composition (delimited respectively by the miscibility-limit and the stability-limit curves), the local supersaturation can lead to the spontaneous nucleation of small particles that subsequently grow or aggregate to form nanoparticles with a very narrow size distribution.[73-76]

Finally, nanoprecipitation can be also described in terms of self-assembling, with particle formation governed by diffusion-limited aggregation of single molecules of the polymer.[26, 52, 77-79] This model has been originally applied to the precipitation of amphiphilic block copolymers, and resembles the micellization process; but in this case it is not reversible, because the formed particles are kinetically frozen, and takes place at higher concentration than usual micellization processes.

A similar approach has been recently proposed also for PCL by Lebouille *et al.*,[80] who proposed a theory based upon a kinetic model for diffusion limited coalescence; the polymer dispersed in a good solvent has originally the size of a swollen coil, but as it is solvated by a bad solvent forms collapsed spheres, which start to coalesce (the particles are considered liquid-like, so they coalesce instead of aggregating). The authors developed analytical expressions to correlate particle size with characteristic mixing and coalescence time, and finally with molar mass and initial polymer concentration, both for the case with and without surfactants. The model predicts that particle diameter scales with 1/3 of the polymer concentration in the slow mixing regime but becomes almost independent in the fast mixing regime limit. MD simulations have confirmed that particle formation can be described by Brownian aggregation of polymer molecules at high polymer concentration: the nanoparticles can be considered amorphous and no energy barrier exists for aggregation.[81]

The previous discussion evidences that it is difficult to establish which is the effective mechanism just looking at the general trends shown by the experimental data. The observed dependence of particle size on initial polymer concentration, in fact, is compatible both with a nucleation-aggregation mecanism and a self assembling one, even if it is difficlt to explain quantitatively the small differences observed in the power law dependence. It can be noted also that the self assembling process in some way resembles homogeneous nucleation, and is often approximated by the expression for homogeneous nucleation kinetics.[78, 79]

Temperature effect might help in discriminating, at least for activated processes, but experimental data at different temperature are lacking; some experiments with PCL and *tert*-

buthanol show no significant temperature effect,[56] but so many parameters weakly depend on it that the interpretation of the results would be difficult.[80]

A multiscale approach, which combines Molecular Dynamics, population balance equations and CFD to describe the precipitation process, can be useful to interpret the experimental data and highligth the role of the different mechanisms, recomposing some of the previously described approaches in a unitary vision. Such a work has been carried out for the nanoprecipitation of PCL from acetone, confirming that different mechanisms may become controlling depending on the operating conditions.[72, 81, 82]

As a general rule, at low polymer concentration (C_{PCL} < 5 mg/mL) a purely aggregative model does not fit the experimental data well, while a nuclation-aggregation model is more effective: from comparison of experimental data and simulations it is possible to infer the the spinodal line which separates the nucleation from the pure aggregation zone may correspond aproximately to a supersaturation of 200. Nucleation-growth mechanisms, with negligible contribution from aggregation, can correctly describe the process only at very low polymer concentration (when the formed particle number is sufficiently low).

The different effect of the three solvents must be explained with different intermolecular interactions between water and solvent; as discussed in the introduction, in the literature it has been observed that the greatest the solvent diffusion coefficient in water and the smallest the nanoparticles formed.

The diffusion coefficients of acetone, acetonitrile and THF are shown in Table 1: it can be observed that solvent-water and water-solvent diffusivity are largely different and change in a different way for the different solvents. As menthol and PCL are initially dissolved in the solvent, it is expected that water-solvent diffusivity be more relevant than solvent-water one for the system under investigation since water must diffuse in the solvent to generate supersaturation. For water-acetonitrile mixtures, water diffusivity in pure acetonitrile was not found in the literature but experimental diffusivity values of water in water-acetonitrile mixtures were reported up to acetonitrile molar fraction 0.75. [64, 83] The values given in Table 1 are a reasonable extrapolation of the trend of water diffusivity in pure acetonitrile.

In this work, water-solvent diffusivities of acetone and acetonitrile are quite similar whereas water-THF diffusivity is smaller: nanoparticle size decreased in the same order as water-solvent diffusivity increase ($D_{w\text{-acetone}} > D_{w\text{-acetonitrile}} > D_{w\text{-THF}}$), and this could be due to faster increase of supersaturation during mixing. Binary water-acetone and water-acetonitrile mixtures have been investigated in several papers:[84-89] both solvents work only as hydrogen-bond acceptors and cannot work as a part of the hydrogen-bonding network of water because

they are not hydrogen bond donors. In other words, both acetone and acetonitrile only experience "additional mixing" rather than "substitutional" mixing in water, which means that the organic molecules exist in the space between water clusters. Nevertheless, despite this similarity, acetone-water and acetonitrile-water solutions present quite a different behaviour: water-acetonitrile solutions are endothermic in the entire concentration range while water-acetone solutions switch from exothermic to endothermic as the molar fraction of acetone exceed 0.5,[88] evidencing significant differences in molecular interactions. Different solvation structures, consequence of differences in the molecular interactions, have been reported also between the water-acetone and the water –THF system.[42, 90]

In this work, as the same volumes of solvent and water were mixed, the resulting molar ratio is 0.24 for acetone, 0.34 for acetonitrile and 0.18 for THF, as far as equilibrium solvent-water mixtures are concerned. In this condition, water-acetone solution shows a negative excess enthalpy of approximately –0.6 kJ/mol [88] while water-acetonitrile solution a positive excess enthalpy of +1 kJ/mol.[89] Thus, water-acetone interactions are enthalpy-controlled while water-acetonitrile interactions are entropy-controlled. A minimum of excess enthalpy is shown for acetone-water at x_{Acetone}=0.20–0.25, which should correspond to the maximum number of hydrogen bonds of acetone-water mixture. Excess enthalpy is correlated with the solvent-water cluster structure,[88] with exothermic solutions forming stable clusters. Acetonitrile-water interactions are not very strong and, when acetonitrile and water are mixed, water preserves its own cluster structure.[83, 89] In the literature, clusters of more than 20 molecules of acetonitrile have been observed in pure acetonitrile and they maintain their structure thanks to dipole-dipole acetonitrile interactions. This scenario suggests that acetonitrile could induce less supersaturation with respect to acetone, which determined slower nucleation. As a consequence nanoparticles grew more in acetonitrile than in acetone.

Of course, excess enthalpy of the binary solutions does not provide the complete picture of the ternary system, which contains PCL also. It is hard to speculate if the different mean size of the nanoparticles is mainly caused by solvent-water interactions or by interaction of the solvent and water molecules with the polymer. It has been confirmed by MD simulations that PCL tends to reside into acetone clusters and clustering of acetone molecules in the vicinity of the polymer chains occurs.[91] Unfortunately, MD simulation of PCL-water plus acetonitrile or THF system are not available and the comparison of the ternary mixture is not possible.

Production of Menthol-Loaded Nanoparticles in CIJM

The picture is much more complex when menthol is added to the system. In fact, as far as the formation mechanisms are concerned, also the nucleation and growth process of the entrapped substance must be considered, and this can be affected by the presence of the polymer: in fact, PCL macromolecules can favor heterogeneous nucleation of the active principle.[92] Moreover, as evidenced by preliminary experiments, menthol-water-acetone system exhibit liquid-liquid phase separation.[61] This phenomenon, called oiling-out, has been reported in the literature when the solute is hydrophobic. In these conditions water, rather than inducing crystallization, promotes the formation of an oily solute-rich organic phase.[93]

TEM analysis confirmed the presence of nanoparticles with different morphologies, as shown in Figure 4: nanoparticles with menthol core and polymer shell, uncomplete or complex structures, but also solid particles.

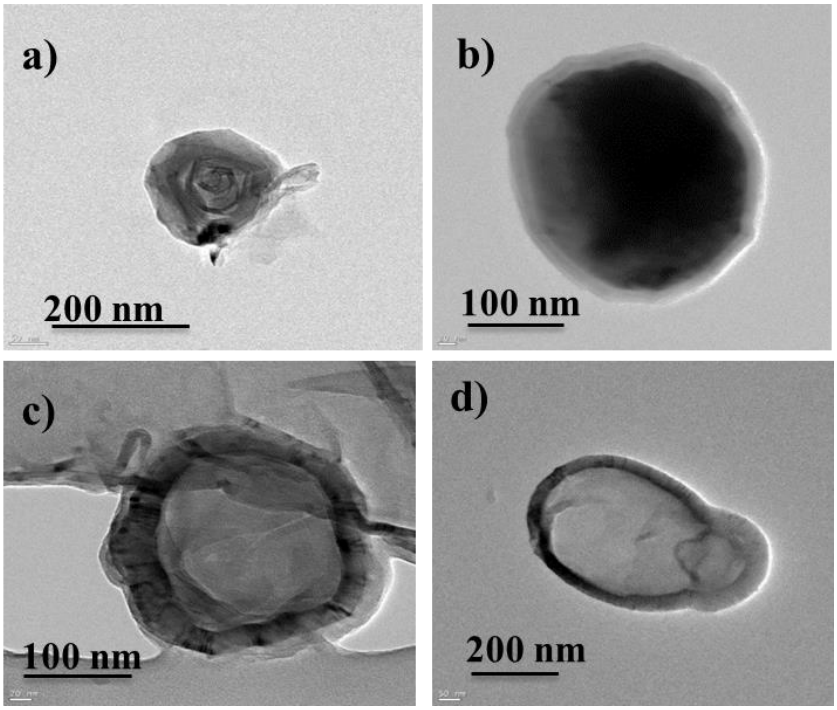

Figure 4. TEM images of polymeric menthol nanoparticles obtained in CIJM; C_{PCL}= 6 mg/mL, *MR*=2, *QR*=1, after centrifugation.

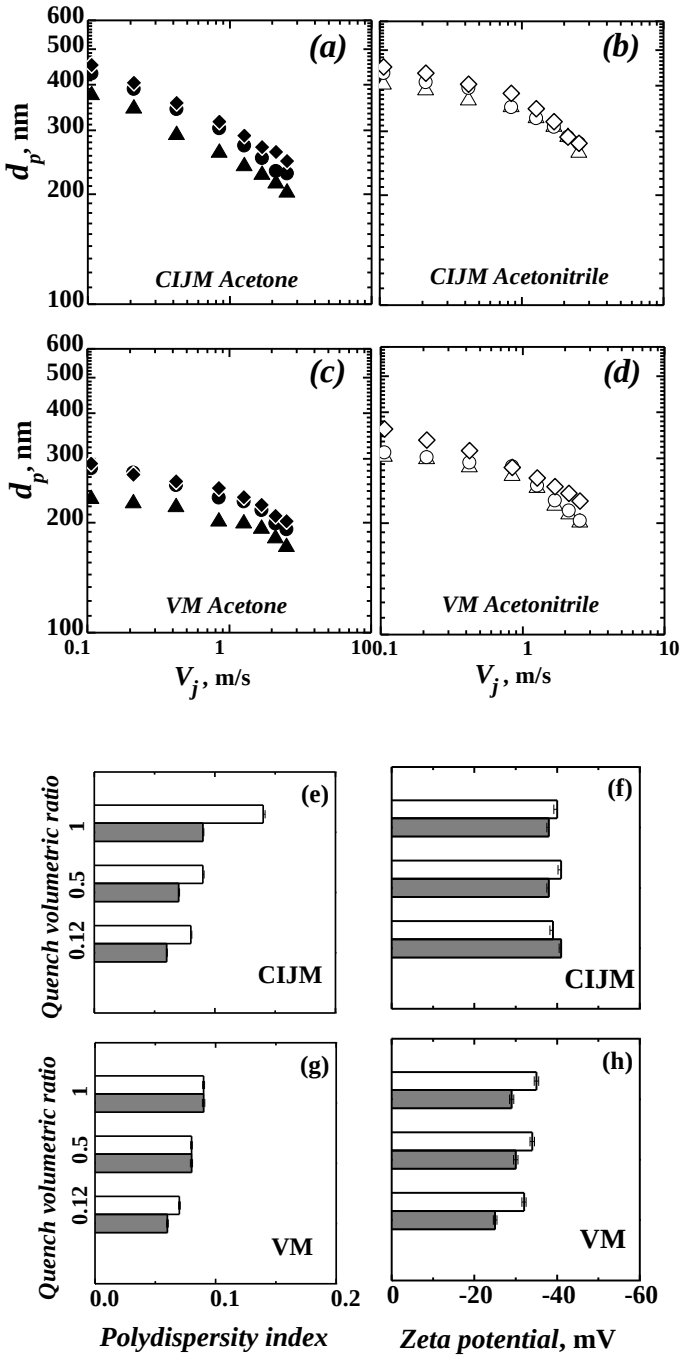

Figure 5. Upper graph block (a-d). Effect of quench ratio on final size of menthol-loaded nanoparticles using acetone (filled symbols, left graphs) and acetonitrile (open symbols, right graphs), in CIJM (upper graphs) and two-inlet VM (lower graphs). Quench ratio, *QR*: ▲,△, 0.12; ●,○, 0.5; ◆,◇, 1.0. Inlet feed, C_{PCL}= 6 mg/mL, *MR*=0.76. The error bars are not shown for sake of clarity.

Lower graph block (e-h). Effect of quench ratio on polydispersity index (PdI) and Zeta potential of menthol-loaded nanoparticles using acetone (grey bars) and acetonitrile (empty bars) in CIJM (upper graphs) and two-inlet VM (lower graphs). Quench ratio, *QR*: 0.12; 0.5; 1.0. Inlet feed, C_{PCL}= 6 mg/mL, *MR*=0.76. Inlet feed velocity *Vj*=1.69 m/s (*FR*= 80 mL/min).

DSC analyses of the nanoparticles were carried out to get information on the physical state of the incorporated menthol (see Figures S2 and S3 in Supplementary Material). The results evidenced that precipitated PCL is partially amorphous, but no distinct peak related to menthol polymorphs could be identified. This can be explained supposing that menthol is in the amorphous phase or dispersed in the polymer matrix; but it must be considered that the degree of cristallinity of a substance incorporated in nanoparticles is very difficult to assess, as a consequence of the strong interaction with the polymer and the small scale.[92]

The effect of solvent on menthol-loaded nanoparticle size was similar to that observed for PCL only (unloaded) nanoparticles, namely the smallest particles were obtained with acetone, larger with acetonitrile and the largest were observed with THF; Figure 5a-b and 6 compare the sizes obtained with the three solvents in CIJM in the range of feed velocities investigated, highligthing also the effect of quench ratio. It can be noted that also the PdI varies in the same way for the three solvents (compare Figure 5e and 6b). Some examples of the reconstitued PSD are shown in Figure S4 (Supplementary material).

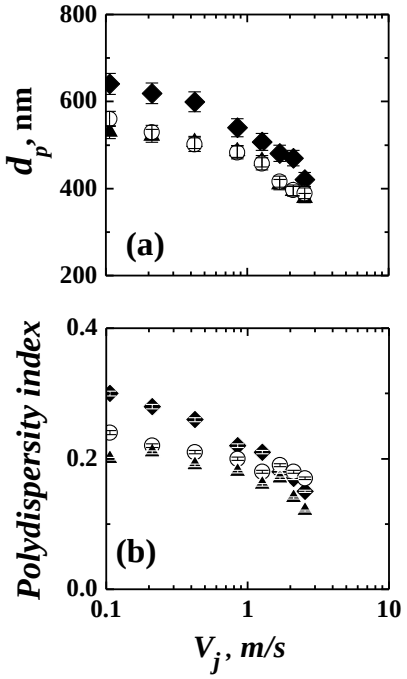

Figure 6. Effect of quench ratio on final size (a) and PdI (b) of menthol-loaded nanoparticles using THF, in CIJM. Quench ratio, *QR*: ▲, 0.12; ○, 0.5; ◆, 1.0. Inlet feed, C_{PCL}= 6 mg/mL, *MR*=0.76.

As mentioned before, immediate dilution in quench water is very important in order to avoid Ostwald ripening, which is proportional to the bulk solubility of the solid,[94] and to limit

further aggregation; this is particularly true if no surfactant is added to the system, as in the present case. The results confirm that *QR* value in the range 0.5-1 is generally a good compromise, and the choice in this range is not critical as the influence on the final size is very limited; but of course the lower the dilution, the more concentrated the suspension, and the easier the further processing. It is worth noting that the curves referring to acetonitrile (Figure 5b-d) are closer to each other than the curves referring to acetone (Figure 5a-c), demonstrating that the effect of quench ratio is less relevant in case of acetonitrile than acetone; in case of THF, a more significant reduction of the final particle size occurs in going from *QR* = 1 to *QR* = 0.5. This trend confirms that quench ratio effect is in relation to PCL solubility in the solvent (which can be estimated in the order $C_{S,THF} > C_{S,acetone} > C_{S,acetnitrile}$) and plays a relevant role especially when polymer solubility in the solvent is high. In fact, experimental data of PCL solubility in acetone and acetonitrile are not available but a rough idea of the relative solubility can be estimated from Hansen solubility parameters [68].

In Table 3 the dispersion, polar and hydrogen bonding contributions as well as the total Hansen solubility parameter are given. Moreover, the distance in the solubility space has been estimated for the pairs PCL-solvent. The greatest the distance, the lower the expected solubility of PCL in the solvent.

Table 3 Solubility parameters of PCL, menthol and solvents.

	δ_D	δ_P	δ_H	δ_T	Distance from PCL*
Water	15.6	16.0	42.3	47.8	35.9
Acetonitrile	15.3	18.0	6.1	24.4	13.8
Acetone	15.5	10.4	7.0	19.9	6.5
THF	16.8	5.7	8.0	19.5	1.0
PCL	17.0	4.8	8.3	19.5	-
Menthol	16.6	4.7	10.6	20.2	2.4

$$*Distance = \left(4(\delta_{d,Solv} - \delta_{d,PCL})^2 + (\delta_{p,Solv} - \delta_{p,PCL})^2 + (\delta_{h,Solv} - \delta_{h,PCL})^2\right)^{\frac{1}{2}}$$

The values in Table 3 confirm that PCL should be more soluble in THF, followed by acetone, acetonitrile and water. Menthol and PCL are very close to each other in terms of solubility parameters, which suggests a good affinity between the two, as testified by the octanol-water partition as well. A recent work from Tian *et al.*[95] proposed the use of solubility paramentes

to design system with improved drug loading and stability and demonstrated that good miscibility between drug and polymer is crucial to high drug loading and stability of the micellar system.

The solubility parameter distance between PCL and water/solvent mixtures is given in Figure 7, with 1:1 water:solvent representing the solution inside the mixer and 2:1 water:solvent the solution after quench (with *QR* =1).

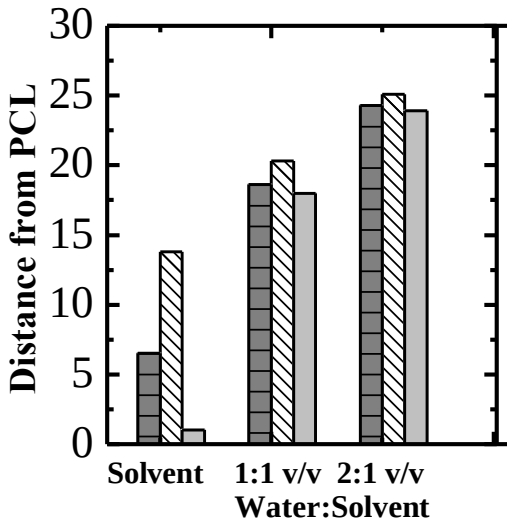

Figure 7. Hansen's solubility parameters distance between PCL and water:solvent mixtures ▤, Acetone; ▨, Acetonitrile; ▩, THF.

Figure 7 highlights that distances between PCL and water/solvent mixtures are levelled off to similar values because of the great distance between PCL and water, which prevails in the weighted average. Therefore, residual PCL solubility in the mixtures should be low and comparable for all solvents. When solvents are mixed in 1:1 volume fraction with water, the PCL distance in the solution increased 18 times with respect to pure solvent for THF, 2.9 times for acetone and only 1.5 times for acetonitrile. However, this information is not correlated with the extent of supersaturation established in the mixer as initial PCL concentration was the same in all solvents and far below solubility limits. On the contrary, the extent of supersaturation should be approximately the same if we assume on the basis of solvent parametes that residual PCL concentration is comparable for all solvents.

The effect of the inlet polymer and menthol concentration on menthol-loaded nanoparticle size is shown in Figure 8 for acetone and acetonitrile.

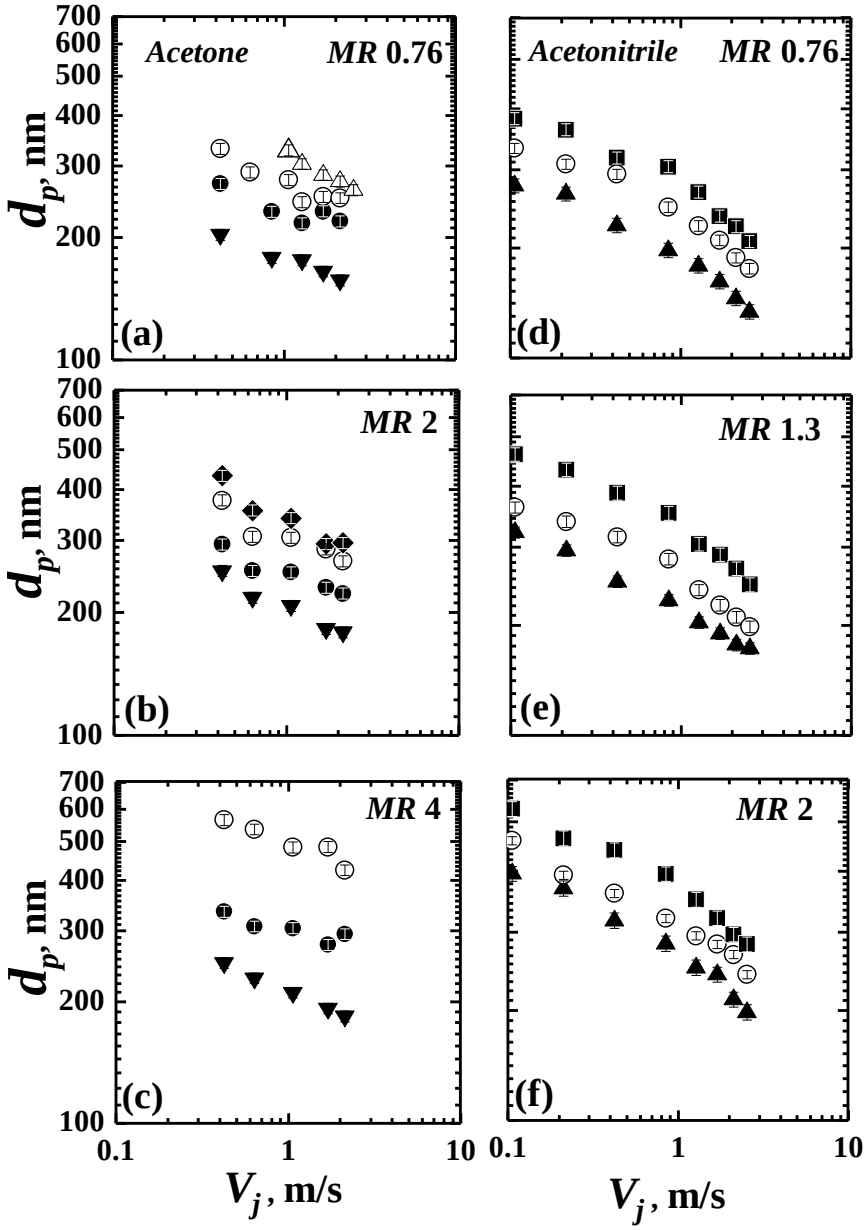

Figure 8. Influence of inlet feed velocity and polymer concentration on menthol-loaded nanoparticle size in CIJM.
Left graphs (a-c): using acetone as solvent, at different menthol to PCL mass ratios; *QR*=1.0. a) *MR*=0.76; b) *MR*=2.0; c) *MR*=4.0. Inlet polymer concentration, C_{PCL}: ▼, 2 mg/mL; ●, 4 mg/mL; ○, 6 mg/mL; ◆, 8 mg/mL; △, 10 mg/mL.
Right graphs (d-f): using acetonitrile as solvent, at different menthol to PCL mass ratios; CIJM, *QR*=0.5. a) *MR*=0.76; b) *MR*=1.3; c) *MR*=2.0. Inlet polymer concentration, C_{PCL}: ▲, 3 mg/mL; ○, 6 mg/mL; ■, 9 mg/mL

In acetone, the influence of hydrodynamics is similar to that observed for PCL only nanoparticles (that is $d_p \propto V_j^{-0.18}$), and the final size is influence by both polymer and menthol inlet concentration. However, the relative influence of polymer and menthol cannot be described by a simple power law. Figure 8 shows the influence of polymer concentration at a

given *MR* ratio (that is for a fixed relative concentration of menthol and PCL): this means that when PCL concentration increases, menthol concentration increases proportionally. It appears that, at a given polymer concentration, the final size is larger at larger *MR* values. Moreover, for a given *MR*, the inlet polymer concentration seems to have a stronger effect in case of unloaded nanoparticles than for menthol-loaded ones; this dependence cannot be easily generalized, anyway, as it is also influenced by the *MR* considered.

A similar complex behaviour had been already reported for polymer nanocapsules containing Miglyol,[48] and may be related to the complexity of the formation process. In fact, it is possible that the two different mechanisms mentioned before as limit cases (nucleation-growth and nucleation-aggregation) act together, with the active principle following mainly a nucleation-growth mechanism (with the possible complication of oiling out and drop coalescence) while the polymer forming the surrounding shell by aggregation or self-assembly. The characteristic time scales of the two processes must match to lead to significant incorporation, and this may justify the observed complex dependence.

Under the same hydrodynamic condition, that is the same feed velocity, the most relevant variables for final particle size was the inlet menthol concentration, as a linear increase was observed, with a weak effect of the relative mass ratio, *MR*. This supports the hypothesis, that we will try to confirm in the next section, that particle size increases with loading, and thus finally loading increases with inlet menthol concentration.

Similar considerations holds also when acetonitrile is used as solvent (Figure 8 right side); as already discussed, the size of the nanacapsules obtained is always larger than with acetone, under the same operating conditions, but the slope of the curves d_p vs V_j in log-log plot suggests that the influence of hydrodynamics is weaker in the laminar or low turbulence regime for acetonitrile than acetone.

An example of the particle size distribution obtained for loaded nanoparticles at different polymer concentration (and constant *MR*) is shown in Figure S5 (Supplementary material); it can be observed that the average size sligthly increases with PCL concentration, but the distribution becomes broader. This was confirmed by the analysis of the polydispersity index (see Figure S6 in Supplementary material) which showed that polydispersity was also significantly affected by the menthol/PCL ratio.

Zeta potential were always in the range between –20 and –50 mV, indicating that the quenched particle are quite stable. Some stability tests confirmed that particle size of supensions stored at ambient temperature did not significantly change for at least 10 days; on the other hand, it was evidenced that much larger particles, in the micrometer range, were

formed with no quench. Non-monomodal distribution, at least at higher inlet concentration, was also observed without quench.[37] Similar values of Zeta potential were obtained for the different solvents (see Figure 5f) but no significant trends were noted, apart for a slight effect of inlet polymer concentration, with more negative values observed at higher concentration (see Figure S6 in Supplementary material). The values observed for loaded and PCL only particles were similar (differences are of the same order of the variations observed for different velocity or polymer concentrations) and no special influence on the measured Zeta potential was also evidenced by the menthol/PCL ratio.

Influence of Mixer Geometry

The CIJM has good performances but some limitations, the main ones are the reduction of mixing performance when unequally flow rates are used, and the relatively high final solvent concentration in the outlet stream (with equal solvent and antisolvent flow rates), which may be responsible for particle growth due to Ostwald ripening. These limitations can be overcome avoiding the direct impingement of the two inlet jets: the simplest configuration to achieve this goal is the vortex mixer, with two tangential inlet streams, a geometry that is preferred to reduce the risk of plugging phenomena, quite common in precipitation reactions. The use of multiple inlets (generally four) allows more freedom in the selection of flow rate and composition of different streams; in all cases the chamber is shallow, usually it has the same height of the inlet tubes, as in the mixers employed in this work.

The mixing performances of the double- [50, 96] and multi-inlet [50] vortex mixer have been investigated in detail by computational fluid dynamics, and it has been confirmed that each stream contributes independently to micromixing in the chamber, as it was supposed in designing this type of mixer. Simulations also confirm that mixing is completed in the main mixing chamber at high Reynolds, while at low Reynolds mixing and reaction can proceed in the outlet tube. Experimental investigations confirm that in the MIVM the flow is turbulent for $Re_j > 240$.[97] CFD results evidence significant differences between the hydrodynamics of the CIJM and MIVM: in the first one, kinetic energy dissipation is maximum in the center of the chamber, while in the vortex mixer the highest turbulent kinetic energy is near its exit, and moves toward the center as Reynolds increases, but for low Re the very center of the chamber has a low kinetic energy. CFD also allowed to evidence mixing performances of VM and MIVM, and of the different MIVM feeding configurations, that is symmetric and non-symmetric, or with only one solvent stream (see Figure 2): the results, and the

experiments with fast mixing-sensitive reactions, suggest slightly better mixing performances for the MIVM with respect to VM, as initially larger segregation length scales can be observed in VM. Minor differences can also be observed for the different inlet configurations: the four streams configuration with equal velocity and symmetrical distribution of the reactants seems more efficient than configurations with unequal stream velocities or unequal reactants distribution.[50]

In spite of the detailed information on hydrodynamics and mixing characteristics of the different mixers, direct comparison of their performances in producing loaded nanoparticles is very limited, and it must be evidenced that the complexity of the mechanisms involved in the synthesis make difficult to predict the influence of mixing quality on final particle size; thus, in this work the three different mixers and the different feeding configurations have been investigated experimentally.

Figures 5c-d show that nanoparticles obtained with the two-streams vortex mixer were smaller compared to those obtained with CIJM, both in acetone and acetonitrile, and polydispersity index had a similar trend (Figure 5g). A similar conclusion was reported for unloaded nanoparticles of a different polymer (a PEGylated derivative of cyanoacrylate) in acetone.[48]

The effect of different feeding configurations is shown in Figure 9 (and Figure S7 in Supplementary material), that also shows the comparison for the two- and four-inlet vortex mixers, both for unloaded and for menthol-loaded nanoparticles. The influence of the solvent in this mixer is the same previously reported for CIJM, with systematically larger particles formed in acetonitrile. Large size differences were observed with different configurations, which were not expected on the base of mixing simulation results: the nanoparticle dimentions obtained in the MIVM mixer were much larger than those obtained in the two-stream VM. Thus, the better mixing performances predicted by CFD for MIVM (and confirmed by model reaction tests), did not result in smaller particles. On the other hand, the symmetric and non-symmetric configuration with two solvent and two antisolvent streams gave similar performances, as predicted by the CFD model, confirming that feeding order is not so important and the mixer is very flexible.

The smallest particles were obtained in the SWWW configuration, which takes advantage of the quench effect directly in the chamber, as the antisolvent flow rate (W) is three times the solvent (S) one. In SWWW configuration no futher dilution was requested, while *QR*=1 was employed in the other cases (SWSW and SSWW). It is worth observing that the final dilution was larger for the MIVM than required for the two-stream VM, even with *QR*=0.5, for

comparable particle sizes. Some significant differences were noted also in the polydispersity index, with higher values for the acetonitrile solvent and the two quenched MIVM configurations.

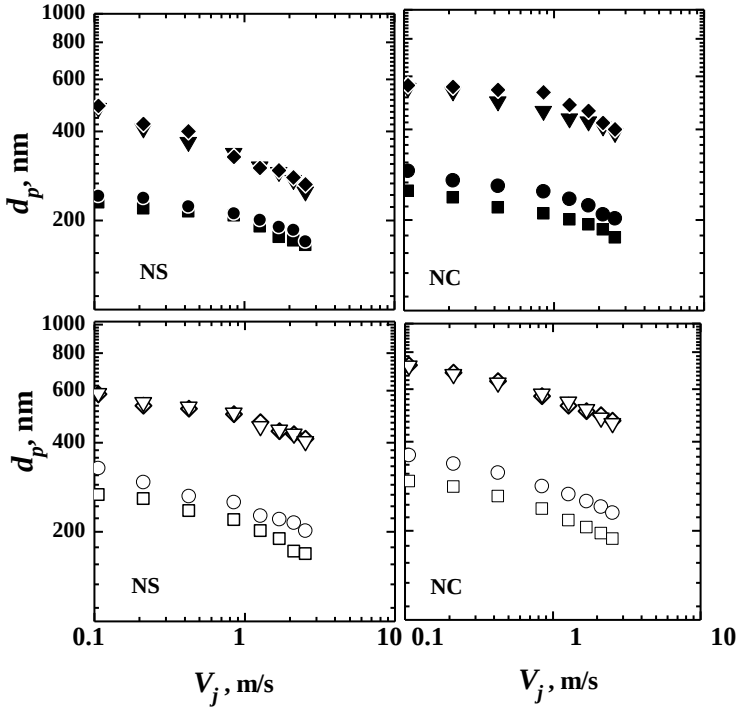

Figure 9. Influence of feed configuration in MIVM on nanaoparticle size, with acetone (filled symbols, upper graphs) and acetonitrile (empty symbols, lower graphs), for PCL only (left graphs) and menthol-loaded PCL nanoparticles (right graphs). Two-streams VM: ●,○ (*QR*=1.0). MIVM: ■,□, SWWW (no quench); ◇,◆, SWSW (*QR*=1.0); ▼,▽, SSWW (*QR*=1). C_{PCL} =6 mg/mL, *MR*=0.76. Error bars are not shown for sake of clarity; see Figure S7 in Supplementary material for PdI and Zeta potential.

As Zeta potential is concerned, differences between the different configurations were small and values observed for loaded and unloaded particles were similar (compare Figure 5f, 5h, S7 in Supplementary material).

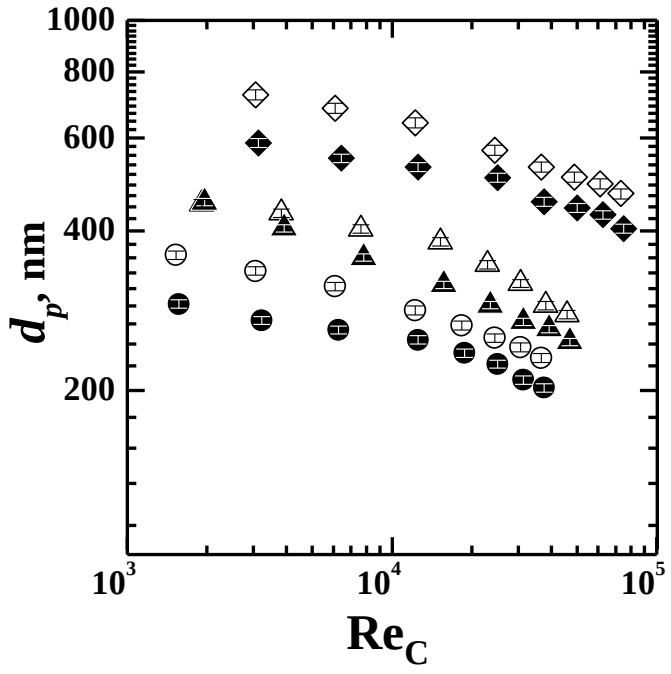

Figure 10. Comparison of mixers performance in term of particle size, using acetone (filled symbols) or acetonitrile (open symbols) as solvent. ●,○, VM; ▲,△, CIJM; ◆,◇, MIVM (SWSW). C_{PCL} =6 mg/mL, *MR*=0.76.

A direct comparison of the three mixers (considering the symmetric feeding configuration for the MIVM) is carried out in Figure 10. To this purpose, the chamber Reynolds number (Re_C) instead of the jet Reynolds number (Re_j) is more convenient for comparison, as suggested in the literature.[50] Re_C, which allows to take into account the different number and flow rate of the various streams, is defined as:

$$\mathrm{Re_C} = \sum_j D_c \frac{\rho_j V_j}{\mu_j} \tag{4}$$

It is evident that VM, CIJM and MIVM gave in the order larger particles; all of them are operating at Re_C>1600, a condition that guarantees full turbulent regime and uniform mixing.[50, 52] Hydrodynamics has still an influence even at Re_C>2000, as the size kept decreasing in the whole investigated range, differently from what reported in literature.[52] To this respect, it must be mentioned that particle size *vs* Reynolds or inlet velocity are quite often plotted in linear scale, in which the strong size variation al low Reynolds is highlighted, while the smaller variations at higher flow rate are poorly evident; the log-log plot evidences that a power-law type relationship still holds, even if changes in slope may occur depending on

change of contribution of different mechanisms, and variations in size in the high turbulent regime are very small in absolute value.

The few available data from literature where a comparison is carried out between CIJM and MIVM confirm that smaller particles are obtained in the CIJM.[52, 53]

Loading and Incorporation Efficiency in the CIJM and MIVM Mixers

As the CIJM and the VM have shown to be suitable for producing nanoparticles in the size range of interest (that is below 500 nm) without excessive dilution (as for the MIVM with a single solvent stream), they were selected for a further investigation of the loading capacity and incorporation efficiency. The results for the two mixers are shown in Figure 11; two different flow rates (20 and 80 mL/min corresponding to 0.42 and 1.69 m/s) were selected to investigate the influence of hydrodynamics on loading. To highlight the effect of menthol and polymer concentration, two PCL concentrations were selected (6 and 12 mg/mL) varying the menthol-to-PCL mass ratio.

Good menthol loadings were obtained, with values ranging from about 40 to 60% in all tested cases. Feeding flow rate and mixer configuration had practically no influence, as the differences were generally of the order of the experimental uncertainty; on the other hand loading increases with menthol-to-polymer mass ratio in the feed, and higher values were observed at lower polymer inlet concentration (which corresponds to smaller particles). It can be noted that particles size increased with loading, and this was higher at higher *MR*, thus confirming that loading increased with inlet menthol concentration. A linear relationship between particle size and loading had been previously reported by Shen *et al.*,[52] for β-carotene encapsulated in PEG-*b*-PCL and by Liu *et al.* [51] for bifenthrin and copolymer stabilizer.

As far as incorporation efficiency is concerned, hydrodynamics and mixer type had practically no influence, and incorporation efficiency was fairly good, with values up to more than 80%, but the influence of polymer and menthol concentration was not straightforward. It is evident from Figure 11 that incorporation efficiency decreased from 80 to 60% by increasing the mass ratios (from 0.76 to 2) at polymer concentration 6 mg/mL. By comparing Figure 11a) and b), it can be observed that at higher menthol concentration (12 mg/mL vs 6 mg/mL) lower encapsulation efficiency were obtained, especially at low *MR* values.

However, the amount of residual menthol in the process solution was not negligible, especially at certain operating conditions, and the issue of menthol separation from the solvent should be addressed.

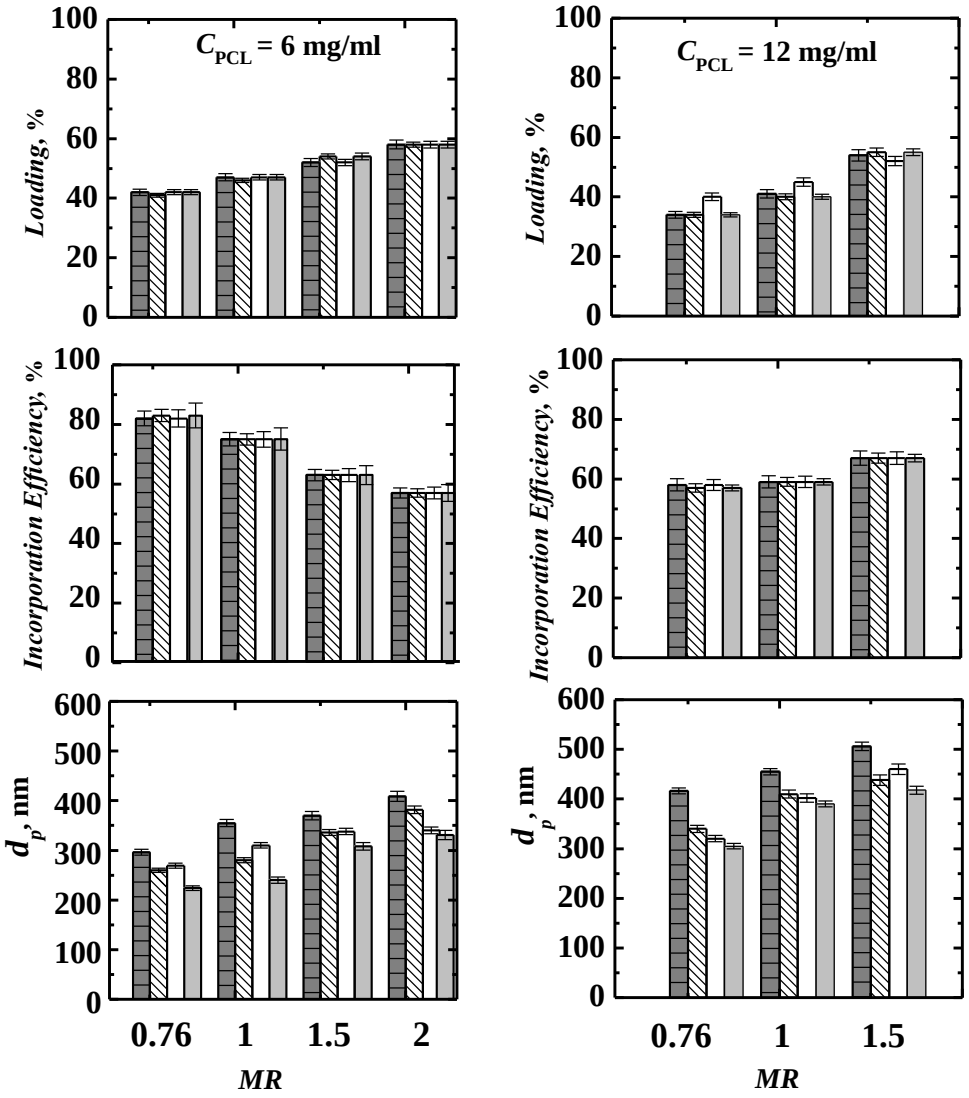

Figure 11. Menthol loading and incorporation efficiency obtained at different inlet PCL concentrations and menthol-to-PCL mass ratio (*MR*) in two mixers (*QR*=1.0). CIJM: ▭, 20 mL/min; ▨; 80 mL/min. VM: □, 20 mL/min; ▭, 80 mL/min.

CONCLUSION

Menthol loaded PCL nanoparticles prepared with both CIJM and vortex mixers were compared. Many parameters (the initial polymer and menthol concentration, mass ratio, quench ratio, inlet feed stream velocity) play a role in the NPs formation process but the most

relevant ones are solvent and mixer type. CIJM produced larger particles than two-stream vortex mixer, and smaller then MIVM. The effect of the solvent had a major impact on the nanoparticle size. Acetone was found to produce the smallest nanoparticle size in comparison to acetonitrile and THF in all the investigated mixers.

Dilution with water, that is quench ratio, is also important in order to achieve nanoparticles with targeted size. As the extent of dilution required is related to the solubility of the polymer in the resulting suspension, the effect of quench ratio is in turn dependent on the solvent type.

The results evidenced a complex dependence of particle size on operating condition, that may be related to the complexity of active mechanisms, which are not fully understood. The contribute of different mechanisms in the formation of polymeric particles and incorporation of an active principle is still an open point, even though simulation work has shown that the controlling mechanism can change in dependence of the operating conditions, such as mixing intensity, species concentration, and possibly temperature (this parameter has been rarely investigated up to now). The presented results can be an experimental set for testing the results of multiscale modelling work extended to different solvents and process conditions.

In a previous work [62] one possible application of menthol-PCL micro and nanoparticles was envisaged in fabric fuctionalization, with the aim of improving wear comfort of compressive stocking. It was proved that menthol-loaded particles distributed on a fabric were effective in giving a refreshing sensation to the wearer through a patch test, and were also evidenced the different performance and role of micro- and nanocapsules. With loading capacities measured in this work, the amount of menthol loaded on one item of clothing can be estimated: the maximum amount of nanoparticles which can be added to the fabric can be estimated in approximately 5 g per square meter (this is a rough value which preserve the fabric characteristics such as stiffness and breathability). Assuming an average LC of 60%, the maximum add-on of menthol on the funtionalized fabric can be approximated to 3 g per square meter.

To favor transdermal release it is important to control the size of the nanoparticles, keeping it below 500 nm; but microparticles in contact with skin can remove an additional amount of heat from the body, contributing to the formulation refreshing effect. In fact, menthol melts close to skin temperature, which is about 33°C on average; in case of phase transition, encapsulation in a polymer shell also avoids leakage of liquid menthol from the formulation..

Latent heat removal is exploited to improve thermal comfort of apparel by means of phase change materials encapsulated in micro sized shells, as discussed by Huang *et al*. in a recent review.[98] Thus, PCL-menthol particles could rely on two different mechanisms to provide

freshness: a transient physical effect due to menthol melting, experienced in a short time after the garment is wore next to skin, and a durable "physiological" effect due to menthol interactions with skin cold receptors.

Acknowledgements.

The main part of the experimental work was carried out by NK who is grateful to Higher Education Commission (HEC) of Pakistan for fully funded PhD scholarship at Politecnico di Torino; RP contributed to experiment and setting procedure for menthol loading evaluation; the contribution to experimental work of T. Zelenková, D. Di Gennaro and P. Rubini is also gratefully acknowledged. The authors are grateful to M. Bazzano for TEM analysis, carried out at Ecole Polytechnique, Laboratoire des Solides Irradies, Paris, under the guidance of Prof. G.Rizza. AF and AAB were responsible for research planning, results interpretation and writing the paper.

Supporting Information

Supplementary material is available.

References

[1] C. Demetzos, *Pharmaceutical Nanotechnology: Fundamentals and Practical Applications*, 1st Edition, Springer Science+Business Media, Singapore **2016**, p. 203.

[2] I. Brigger, C. Dubernet, P. Couvreur, *Adv. Drug Deliv. Rev.* **2002**, *54* (5), 631.

[3] US5118528A (1992), Centre National De La Recherche Scientifique, Invs: C. Fessi, J.-P. Devissaguet, F. Puisieux, C. Thies.

[4] S. Galindo-Rodriguez, E. Allémann, H. Fessi, E. Doelker, *Pharm. Res.* **2004**, *21* (8), 1428.

[5] M.P. Desai, V. Labhasetwar, G.L. Amidon, R.J. Levy, *Pharm. Res.* **1996**, *13* (12), 1838.

[6] G. Nelson, *Int. J. Pharm.* **2002**, *242* (1–2), 55.

[7] K. S. Paudel, M. Milewski, C. L. Swadley, N. K. Brogden, P. Ghosh, A. L. Stinchcomb, *Ther. Deliv.* **2010**, *1* (1), 109.

[8] O. Uchechi, J. D. N. Ogbonna, A. A. Attama, "Nanoparticles for Dermal and Transdermal Drug Delivery," *Application of Nanotechnology in Drug Delivery*, A. D. Sezer, Ed., InTech **2014**, DOI: 10.5772/58672, p. 193.. Available from: http://www.intechopen.com/books/application-of-nanotechnology-in-drug-delivery/nanoparticles-for-dermal-and-transdermal-drug-delivery.

[9] J. J. Escobar-Chávez, R. Díaz-Torres, I. M. Rodríguez-Cruz, C. L. Domínguez-Delgado, R. S. Morales, E. Ángeles-Anguiano, L. M Melgoza-Contreras, *Res. Rep. Transderm. Drug Deliv.* **2012**, *1* (1), 3.

[10] R. Eccles, *J. Pharm. Pharmacol.* **1994**, *46* (8), 618.

[11] B. Harris, *Int. J. Aromather.* **2006**, *16*-(3–4), 117.

[12] D. D. McKemy, W. M. Neuhausser, D. Julius, *Nature* **2002**, *416*, 52.

[13] A. M. Peier, A. Moqrich, A. C. Hergarden, A. J. Reeve, D. A. Andersson, G. M. Story, T. J. Earley, I. Dragoni, P. McIntyre, S. Bevan, A. Patapoutian, *Cell* **2002**, *108*, 705.

[14] T. Patel, Y. Ishiuji, G. Yosipovitch, *J. Am Acad. Dermatol.* **2007**, *57* (5), 873.

[15] G. Yener, U. Gonullu, M. Uner, T. Degim, A. Araman, *Pharmazie* **2003**, 58, 330.

[16] P. A. Cornwell, B. W. Barry, C. P. Stoddart, J. A. Bouwstra., *J. Pharm. Pharmacol.* **1994**, *46*, 938.

[17] K. Cal, S. Janicki, M. Sznitowska, *Int. J. Pharm.* **2001**, *224*, 81.

[18] M. Elsabahy, K. L. Wooley, *Chem. Soc. Rev.* **2012**, *41* (7), 2545.

[19] S. S . Guterres, M. P. Alves, A. R. Pohlmann, *Drug Target Insights* **2007**, *2* (2), 147.

[20] A. Kumari, S. K. Yadav, S. C. Yadav, *Coll. Surf. B: Biointerfaces* **2010**, *75*, 1.

[21] D. Horn, J. Rieger, *Ang. Chemie Int. Ed.* **2001**, *40* (23), 4330.

[22] J. W. Chung, K. Lee, C. Neikirk, C. M. Nelson, R. D. Priestley, *small* **2012**, *8* (11), 1693.

[23] G.S. Kwon, T., Okano Polymeric micelles as new drug carriers, *Adv. Drug Deliv. Rev.* **1996**; *21* (2), 107.

[24] D. Sutton, N. Nasongkla, E. Blanco, J. Gao, *Pharm. Res.* **2007**, *24* (6):1029.

[25] Y. Zhang, Y. Huang, S., *AAPS PharmSciTech*. **2014**, *15* (4), 862.

[26] B. K. Johnson, R. K. Prud'homme, *Aust. J. Chem.* **2003**, *56* (10), 1021.

[27] D. Quintanar-Guerrero, E. Allémann, H. Fessi, E. Doelker, *Drug Dev. Ind. Pharm.* **1998**, *24* (12), 1113.

[28] B. V. N. Nagavarma, K. S. Y. Hemant, A. Ayaz, L. S. Vasudha, H. G. Shivakumar, *Asian J. Pharm. Clin. Res.* **2012**, *5* (3), 16.

[29] B. B. C. Youan, M.-A. Bendit, B. Baras, J. Gillard, *J. Microencapsul.* **1999**, 16 (5), 587.

[30] E. Merisco-Liversidge, G. G. Liversidge, E. R. Cooper, *Eur.. J. Pharm. Sci.* **2003**, *18* (2), 113.

[31] H. Fessi, J. P. Puisieux, N. Devissaget, N. Ammoury, S. Benita, *Int. J. Pharm.* **1989**, 5 (1), 1.

[32] M. Ben Yehuda Greenwald, S. Ben Sasson, H. Bianco-Peled, *J. Microencapsul.* **2013**, *30* (6), 580.

[33] A.-L. Le Roy Boehm, R. Zerrouk, H. Fessi, *J. Microencapsulation* **2000**, *17*, 195.

[34] C. Zhang, V. J. Pansare, R. K. Prud'homme, R. D. Piestley, *Soft Matter* **2012**, *8*, 86.

[35] N. Di Pasquale, D. L. Marchisio, A. A. Barresi, *Chem. Eng. Sci*. **2012**, 84, 671.

[36] A. Mersmann, *Chem. Eng. Proc.* **1999**, *71* (11), 1240.

[37] A. A. Barresi, M. Vanni, D. Fissore, T. Zelenková, "Synthesis and Preservation of Polymer Nanoparticles for Pharmaceuticals Applications," *Handbook of Polymers for Pharmaceutical Technologies* – Vol. 2: *Processing and Applications*, 1st Edition, V. K. Thakur, M. K. Thakur, Eds., John Wiley & Son s Inc, Hoboken (New Jersey) and Scrivener Publishing I.I.C., Salem (Massachussetts) **2015**, p. 229.

[38] W. S. Saad, R. K. Prud'homme, *Nano Today* **2016**, *11*, 212.

[39] B. K. Johnson, R. K. Prud'homme, *AIChE J.* **2003**, 49 (9), 2264.

[40] D. L. Marchisio, L. Rivautella, A. A. Barresi, *AIChE J.* **2006**, *52* (5), 1877.

[41] F. Lince, D. L. Marchisio, A. A. Barresi, *J. Colloid Interf. Sci*. **2008**, *332* (2), 505.

[42] F. Lince, S. Bolognesi, D. L. Marchisio, B. Stella, F. Dosio, A. A. Barresi, L. Cattel, *J. Pharm. Sci.* **2011**, *100* (6), 2391.

[43] A. A. Thorat, S. V. Dalvi, *Chem. Eng. J.* **2012**, *181–182*, 1.

[44] F. Lince, *Preparation and Characterization of Polymeric Nanoparticles for Pharmaceutical Applications*, PhD Thesis, Politecnico di Torino, Torino, Italy **2010**, p. 194.

[45] F. Lince, D. L. Marchisio, A. A. Barresi, *Chem. Eng. Process.* **2011**, *50* (4), 356.

[46] E. Gavi, D. L. Marchisio, A. A. Barresi, *Chem. Eng. Sci*. **2007**, *62* (8), 2228.

[47] F. Lince, D. L. Marchisio, A. A. Barresi, *Chem. Eng. Res. Des.* **2009**, *87* (4), 543.

[48] I. Valente, E. Celasco, D. L. Marchisio, A. A. Barresi, *Chem. Eng. Sci.* **2012**, ***77***, 217.

[49] T. Zelenková, D. Fissore, D. L. Marchisio, A. A. Barresi,. *J. Pharm. Sci.* **2014**, *103* (6), 1839.

[50] Y. Liu, C. Cheng, Y. Liu, R. K. Prud'homme, R. O. Fox, *Chem. Eng. Sci.* **2008**, *63* (11), 2829.

[51] Y. Liu, Z. Tong, R. K. Prud'homme, *Pest Manag. Sci.* **2008**, 64 (8), 808.

[52] H. Shen, S. Hong, R. K. Prudhomme, Y. Liu, *J. Nanop. Res*. **2011**, *13* (9), 4109.

[53] J. Han, Z. Zhu, H. Qian, A. R. Wohl, C. J. Beaman, T. R. Hoye, C. W. Macosko, *J. Pharm. Sci.* **2012**, *101* (10), 4018.

[54] F. Chow, C. C. Sun, A. H. L. Chow, *Eur. J. Pharm. Biopharm.* **2014**, *88* (2), 462.

[55] U. Bilati, E. Allémann, E. Doelker, *Eur. J. Pharm. Sci*. **2005**, *24* (1), 67.

[56] T. Zelenková, A. A. Barresi, D. Fissore, *J. Pharm. Sci*. **2015**, *104* (1), 178.

[57] C. G. Pitt, A. R. Jeffcoat, R. A. Zweidinger, A. Schindler, *J. Biomed. Mat. Res*. **1979**, *13*, 497.

[58] C. G. Pitt, M. M. Gratzl, A. R. Jeffcoat, R. A. Zweidinger, A. Schindler, *J. Pharm. Sci.* **1979**, *68*, 1534.

[59] V. R. Sinha, K. Bansal, R. Kaushik, R. Kumria, A. Trehan, *Int. J. Pharm.* **2004**, *278* (1), 1.

[60] R. Peila, A. Ferri, M. Mihailiasa, A. A. Barresi, T. Zelenkova, I. Bevilacqua, A. Musinguzi, "Study on transdermal release from functionlized cotton fabrics with caffeine-polycaprolactone nanocapsules," *Proc. Ambience14&10i3m "Scientific Conference for Smart and Functional Textiles, Well-Being, Thermal Comfort in Clothing, Design, Thermal Manikins and Modelling* (M. Varheenmaa, Ed.), University of Helsinki, Tampere, Finland, 7-9 September **2014**, paper ID230.

[61] A. Ferri, R. Peila, N. Kumari, M. Mihailiasa, A. Barresi, "Encapsulation of active principles in PCL for knitted fabrics functionalization," *20th International Symposium on Microencapsulation IMS2015*, Boston, MA, USA, 1-3 October **2015**.

[62] R. Mossotti, A. Ferri, R. Innocenti, T. Zelenková, F. Dotti, D. L. Marchisio, A. A. Barresi, *J. Microencapsul.* **2015**, *32* (7), 650.

[63] K. H. Hellwege, Ed., *Landolt-Bornstein, Numerical Data and Functional Relationship in Science and Technology*, 6th Edition, Vol II/5a, *Transport Phenomena (Viscosity and Diffusion)*, Springer-Verlag, Heidelberg, **1969.**

[64] A. M. Nikitin, A. P. Lyubartsev, *J. Comp. Chem.* **2007**, *28* (12), 2020.

[65] S. H. Donaldson, J. P. Jahnke, R. J. Messinger, A. Östlund, D. Uhrig, J. N. Israelachvili, B. F. Chmelka, *Macromol.* **2016**, *49* (18), 6910.

[66] M. Okuniewski, K. Paduszyński, U. Domańska, *Fluid Phase Equilibria* **2016**, *422*, 66.

[67] T. Zelenkova, *Production and Preservation of Poly-ε-caprolactone Nanoparticles*. PhD Thesis, Politecnico di Torino, Italy **2015**, p. 130. Available at http://porto.polito.it/id/eprint/2588570.

[68] C. Bordes, V. Fréville, E. Ruffin, P. Marote, J. Y. Gauvrit, S. Briançon, P. Lantéri, *Int. J. Pharm.* **2010**, *383* (1–2), 236.

[69] L. Zhu, H. Lan, B. He, W. Hong, J. Li, *Int. J. Chem. Eng.* **2010**, *2010*, Article ID 608680, doi:10.1155/2010/608680.

[70] M. Icardi, E. Gavi, D. L. Marchisio, A. A. Barresi, M. G. Olsen, R. O. Fox, D. Lakehal, *Chem. Eng. J.* **2011**, *166* (1), 294–305.

[71] Y. Singh, P.Ojha, M. Srivastava, M. K. Chourasia,. Reinvestigating nanoprecipitation via Box-Behnken design: a systematic approach. *J. Microencapsulation* **2015**, *32*, 75-85.

[72] N. Di Pasquale, D. L. Marchisio, P. Carbone, A. A. Barresi, *Chem. Eng. Res. Des*. **2013**, *91* (11), 2275.

[73] J. Aubry, F. Ganachaud, J. P. C. Addad, B. Cabane, *Langmuir* **2009**, *25*, 1970.

[74] S. A. Vitale, J. L. Katz, *Langmuir* **2003**, *19* (10), 4105.

[75] F. Ganachaud, J. L. Katz, *ChemPhysChem* **2005**, *6* (2), 209.

[76] M. Beck-Broichsitter, E. Rytting, T. Lebhardt, X. Wang, T. Kissel, *Europ. J. Pharm. Sci*. **2010**, *41* (2), 244.

[77] B.K. Johnson, R. K. Prud'homme, *Phys. Rev. Lett.* **2003**, *91* (11), article 118302.

[78] J. C. Cheng , R. D. Vigil, R. O. Fox., *J Colloid Interf. Sci.* **2010**, *351* (2), 330.

[79] J. C. Cheng, R. O., *Ind. Eng. Chem. Res.* **2010**, *49* (21), 10651.

[80] J. G. J. L. Lebouille, R. Stepanyan, J. J. M. Slot, M. A. Cohen Stuart, R. Tuinier, *Colloids Surf. A: Phys. Eng Asp*. **2014**, *460*, 225.

[81] A. D. Lavino, N. Di Pasquale, P. Carbone, A.A. Barresi, L. D.Marchisio, 2015, "Simulation of macromolecule self-assembly in solution: a multiscale approach," *Polymer Processing with Resulting Morphology and Properties: Feet in the Present and Eyes at the Future. Proceedings of the GT70 International Conference*, Salerno, Italy, 15-17 October **2015**. *AIP Conf. Proc*. 1695 (R. Pantani , V. Speranza, F. De Santis, eds.), article nr. 020036.

[82] A. Lavino, N. Di Pasquale, P. carbone, D. L. Marchisio, A novel multiscale model for the simulation of polymer flash nanoprecipitation, *Chem. Eng. Sci*. **2017** (submitted).

[83] T. Takamuku, M. Tabata, A. Yagamuchi, J. Nishimoto, M. Kumamoto, H. Wakita, T. Yamaguchi, *J. Phys. Chem. B* **1998**, *102* (44), 8880.

[84] S. Weerasinghe, P. E. Smith, *J. Chem. Phys.* **2003**, *118* (23), 10663.

[85] A. Perera, F. Sokolić, *J. Chem. Phys.* **2004**, *121* (22), 11272.

[86] S. M. Hurley, T. E. Dermota, D. P. Hydutsky, A. W. Jr. Castleman, *Int. J. Mass Spectrom*. **2003**, *228* (2-3), 677.

[87] I. V. Hertel, W. Radloff, *Rep. Prog. Phys.* **2006**, *69* (6), 1897.

[88] R. G. Pereyra, M. L. Asar, M. A. Carignano, *Chem. Phys. Lett*. **2011**, *507* (4-6), 240.

[89] A. Wakisaka, H. Abdoul-Carime, Y. Yamamoto, Y. Kiyozumi, *J. Chem. Soc. Faraday Trans.* **1998**, *94* (3), 369.

[90] M. Katayama, K. Ozutsumi, J. *Sol. Chem.* **2008**, *37* (6), 841.

[91] N. Di Pasquale, D. L. Marchisio, A. A. Barresi, P. Carbone, *J. Phys. Chem. B* **2014**, *118* (46), 13258.

[92] S. M. D'Addio, R. K. Prud'homme, *Adv. Drug Del. Rev.* **2011**, *63*, 417.

[93] I. de Albuquerque, M. Mossotti, *Cryst. Grow. and Des.* **2014,** *14*, 5617.

[94] B. Wang, R. Finsy, H. B. Xu, X. Li, *J. Zhejiang Univ. Sci.* **2005**, (8), 705.

[95] Y. Tian , C. Shi, Y. Sun, C. Zhu, C. C. Sun, S. Mao, *Mol. Pharm.* **2015**,12(3),816.

[96] D. L. Marchisio, F. Omegna, A. A. Barresi, P. Bowen, *Ind. Eng. Chem. Res.* **2008**, *47* (19), 7202.

[97] Y. Shi, J. C. Cheng, R. O. Fox, M. G. Olsen, *J. Micromech Microeng.* **2013**, *23* (7), article 075005.

[98] X. Huang, G. Alva, Y. Jia, G. Fan, *Renew. Sust. Energy Rev.* **2017**, *72*, 128.

List of Symbols

C_{PCL}	poly-ε-caprolactone concentration (kg/m^3)
C_S	saturation concentration
D	diffusivity (m^2/s)
D_c	chamber diameter (m)
d_{in}	inlet jet diameter (m)
d_{out}	outlet jet diameter (m)
d_p	mean nanoparticle diameter (m)
MR	mass ratio between menthol and PCL concentration
QR	quench ratio
Re_C	chamber Reynolds number
Re_j	jet Reynolds number
x	molar fraction
V_j	inlet jet velocity (m/s)

Greek letters

α	exponent in power law relationship, Equation (3)
β	exponent in power law relationship, Equation (3)
δ	Hansen solubility parameter
μ	viscosity (Pa·s)
ρ	density (kg/m^3)

Abbreviations

API	Active principle ingredient
CIJM	Confined impinging jet mixer
CFD	Computational Fluid Dynamics
DLS	Dynamic Light Scattering
DSC	Differential Scanning Calorimetry
GC	Gaschromatograph
IE	Incorporation Efficiency, Equation (2)
LC	Loading Capacity, Equation (1)
MD	Molecular Dynamics
MIVM	Multi inlet vortex mixer (four inlet streams)

NP	Nanoparticle
NS	Nanosphere
PCL	Poly-ε-caprolactone
PdI	Polydispersity Index
PSD	Particle Size Distribution
TEM	Trasmission Electron Microscopy
THF	Tetrahydrofuran
VM	Vortex mixer (two inlet streams)

Table headings

Table 1. Physicochemical data of organic solvents used for nanoparticle synthesis at 25ºC.

Table 2. Operating conditions in the CIJM and vortex mixers.

Table 3. Solubility parameters of PCL, menthol and solvents.

Captions for figures

Figure 1. Sketch of the confined impinging jet mixer (CIJM) used for the preparation of nanoparticles. (d_{in} = 1 mm, d_{out} = 2 mm, D_c = 5 mm, total chamber height = 11.2 mm).

Figure 2. Tested feeding configurations for the vortex mixer with four and two feeding streams. d_{in}= 1 mm, d_{out}= 2 mm, D_c = 4 mm. PCL and menthol were always fed together in the solvent streams.

Figure 3. Influence of inlet feed velocity and polymer concentration on PCL only (unloaded) particles size, Polydispersity index (PdI) and zeta potential, using acetone (filled symbols) and acetonitrile (open symbols). Inlet polymer concentration, C_{PCL}: ■,□, 3 mg/mL; ▲,△, 6 mg/mL; ◆,◇, 9 mg/mL. *QR*=0.5. CIJM mixer.

Figure 4. TEM images of polymeric menthol nanoparticles obtained in CIJM; C_{PCL}= 6 mg/mL, *MR*=2, *QR*=1, after centrifugation.

Figure 5. Upper graph block (a-d). Effect of quench ratio on final size of menthol-loaded nanoparticles using acetone (filled symbols, left graphs) and acetonitrile (open symbols, right graphs), in CIJM (upper graphs) and two-inlet VM (lower graphs). Quench ratio, *QR*: ▲,△, 0.12; ●,○, 0.5; ◆,◇, 1.0. Inlet feed, C_{PCL}= 6 mg/mL, *MR*=0.76. The error bars are not shown for sake of clarity.

Lower graph block (e-h). Effect of quench ratio on polydispersity index (PdI) and Zeta potential of menthol-loaded nanoparticles using acetone (grey bars) and acetonitrile (empty bars) in CIJM (upper graphs) and two-inlet VM (lower graphs). Quench ratio, *QR*: 0.12; 0.5; 1.0. Inlet feed, C_{PCL}= 6 mg/mL, *MR*=0.76. Inlet feed velocity *Vj*=1.69 m/s (*FR*= 80 mL/min).

Figure 6. Effect of quench ratio on final size (a) and PdI (b) of menthol-loaded nanoparticles using THF, in CIJM. Quench ratio, *QR*: ▲, 0.12; ○, 0.5; ◆, 1.0. Inlet feed, C_{PCL}= 6 mg/mL, *MR*=0.76.

Figure 7. Hansen's solubility parameters distance between PCL and water:solvent mixtures ▤, Acetone; ▨, Acetonitrile; ■, THF.

Figure 8. Influence of inlet feed velocity and polymer concentration on menthol-loaded nanoparticle size in CIJM.
Left graphs (a-c): using acetone as solvent, at different menthol to PCL mass ratios; *QR*=1.0. a) *MR*=0.76; b) *MR*=2.0; c) *MR*=4.0. Inlet polymer concentration, C_{PCL}: ▼, 2 mg/mL; ●, 4 mg/mL; ○, 6 mg/mL; ◆, 8 mg/mL; △, 10 mg/mL.
Right graphs (d-f): using acetonitrile as solvent, at different menthol to PCL mass ratios; CIJM, *QR*=0.5. a) *MR*=0.76; b) *MR*=1.3; c) *MR*=2.0. Inlet polymer concentration, C_{PCL}: ▲, 3 mg/mL; ○, 6 mg/mL; ■, 9 mg/mL

Figure 9. Influence of feed configuration in MIVM on nanaoparticle size, with acetone (filled symbols, upper graphs) and acetonitrile (empty symbols, lower graphs), for PCL only nanospheres (NS, left graphs) and menthol-loaded nanoparticles (NC, right graphs). Two-streams VM: ●,○ (*QR*=1.0). MIVM: ■,□, SWWW (no quench); ◇,◆, SWSW (*QR*=1.0); ▼,▽, SSWW (*QR*=1). C_{PCL} =6 mg/mL, *MR*=0.76. Error bars are not shown for sake of clarity; see Figure S7 in Supplementary material for PdI and Zeta potential.

Figure 10. Comparison of mixers performance in term of particle size, using acetone (filled symbols) or acetonitrile (open symbols) as solvent. ●,○, VM; ▲,△, CIJM; ◆,◇, MIVM (SWSW). C_{PCL} =6 mg/mL, *MR*=0.76.

Figure 11. Menthol loading and incorporation efficiency obtained at different inlet PCL concentrations, menthol-to-PCL mass ratio (*MR*) in two mixers (*QR*=1.0). CIJM: ▤, 20 mL/min; ▨; 80 mL/min. VM: □, 20 mL/min; ■, 80 mL/min.

Production of menthol-loaded nanoparticles by solvent displacement

Ferri A.*, Kumari N., Peila R. and Barresi A. A.

Department of Applied Science and Technology, Politecnico di Torino
Corso Duca degli Abruzzi 24, 10129 Torino (Italy)

Supplementary material

to the article published in

Canadian Journal Chemical Engineering

(special issue GRICU 2016)

filed with: Depository for Unpublished Data, CISTI,
National Research Council Canada, Ottawa, Ontario, Canada K1A 0S2

* Corresponding author.

Chemicals

The main physical properties of menthol are reported in Table S1.

Table A1 Chemico-physical properties of racemate menthol.

Molecular weight (g/mol)	156.27
Melting temperature (°C)	30-32
Density (kg/m^3)	895
LogK_{ow}	3.4
$\Delta H_{melting}$ (kJ/mol)	10.25–12.83
Vapour pressure (hPa)	0.085 at 25°C

Influence of solvent type on nanoparticle size

The results confirm that the particle size decreased with increasing feed velocity and increased with increasing polymer concentration: the trend can be described by a power-law equation, at least in the turbulent range for Re_j>310. The trend is similar for acetone, acetonitrile and THF, but particles are significantly larger than in acetone at the same operating conditions (see a direct comparison in Figure S1).

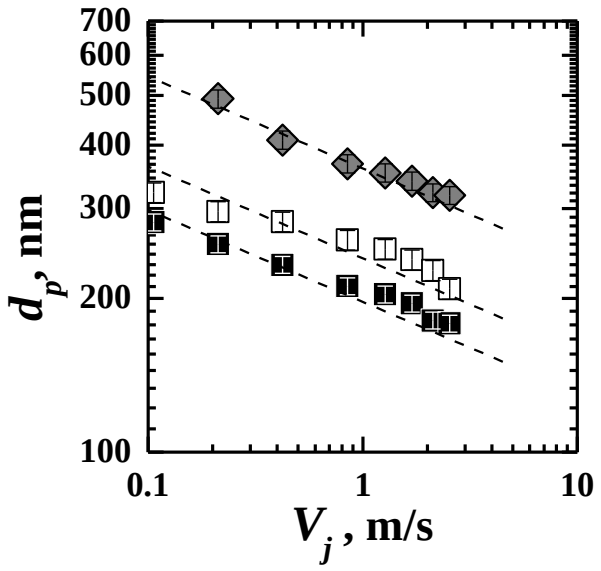

Figure S1. Influence of different solvents and inlet feed velocity on PCL only particles size: ■, acetone; □, acetonitrile; ◆, THF. Inlet polymer concentration, C_{PCL}: 3 mg/mL; *QR*=0.5. CIJM mixer. Trend line have been calculated using Eq. (3) with β= – 0.18.

Particle characterization: DSC analysis

Figure S2 shows the thermographs of the pure substances, for reference. The two polymorphs of menthol racemic mixture melts at 28°C and 38°C respectively: only a very minor fraction of the first one is present in the material as received, while the main melting peak of menthol is observed at 38°C. If the sample is previously premelted at 40°C and cooled, different melting peaks appear, corrispondent to different polymorphs.

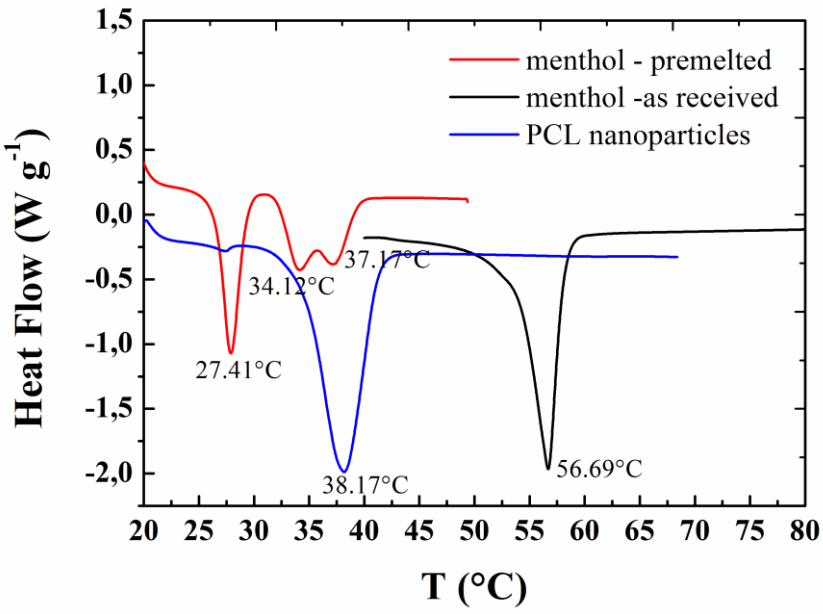

Figure S2. DSC thermograph of menthol and PCL nanoparticles (C_{PCL} = 25 mg/mL); menthol was analysed as received and after melting and solidification. Heating rate: 5°C/min

PCL dissolved in acetone and precipitated in the CIJM (without any menthol) shows a melting temperature around 56°C (experimental data in different samples range from 55.7 to 56.7°C); rapid precipitation from the solvent freezes the PCL structure in a partially amorphous arrangement, as confirmed by the evaluation of the melting enthalpy [theoric PCL melting enthalpy is 134.9 kJ/kg (C. G. Pitt, *Drugs Farm. Sci*. **1990**, 45, 71)].
Figure S3(a) shows a cyclic thermograph of another sample of PCL nanoparticles; in this case the sample is first heated up to 100°C and melted, cooled to 20°C (it can be seen that crystallisation takes place) and then heated up again, always at 5°C/min. It can be noted that the PCL main melting peaks is slightly shifted at lower temperature in the second cycle, which confirms that the melting temperature is affected by the degree of crystallinity and thus by the formation conditions.
A thermograph of loaded nanoparticles is shown in Figure S3(b); it appears very similar to that of pure PCL, as it does not show any menthol melting peak, but only a single melting peak practically at the same temperature of pure precipitated PCL. Samples of NPs prepared in different conditions showed very similar thermographs. This confirms that the encapsulated menthol is either dispersed in the amorphous fraction of PCL, or it forms an amorphous core in the nanoparticles
Some tests have been carried out holding the sample at 40°C, before cooling it to 25°C and heating at 5°C/min (see R. Mossotti et al., *J. Microencapsul.* **2015**, *32* (7), 650). These DSCs resulted different from the previous ones, as melting peaks at different temperature appeared;

they are difficult to be interpreted, because the peak temperatures vary depending on the inlet polymer and menthol concentrations, but confirm the encapsulation of menthol.

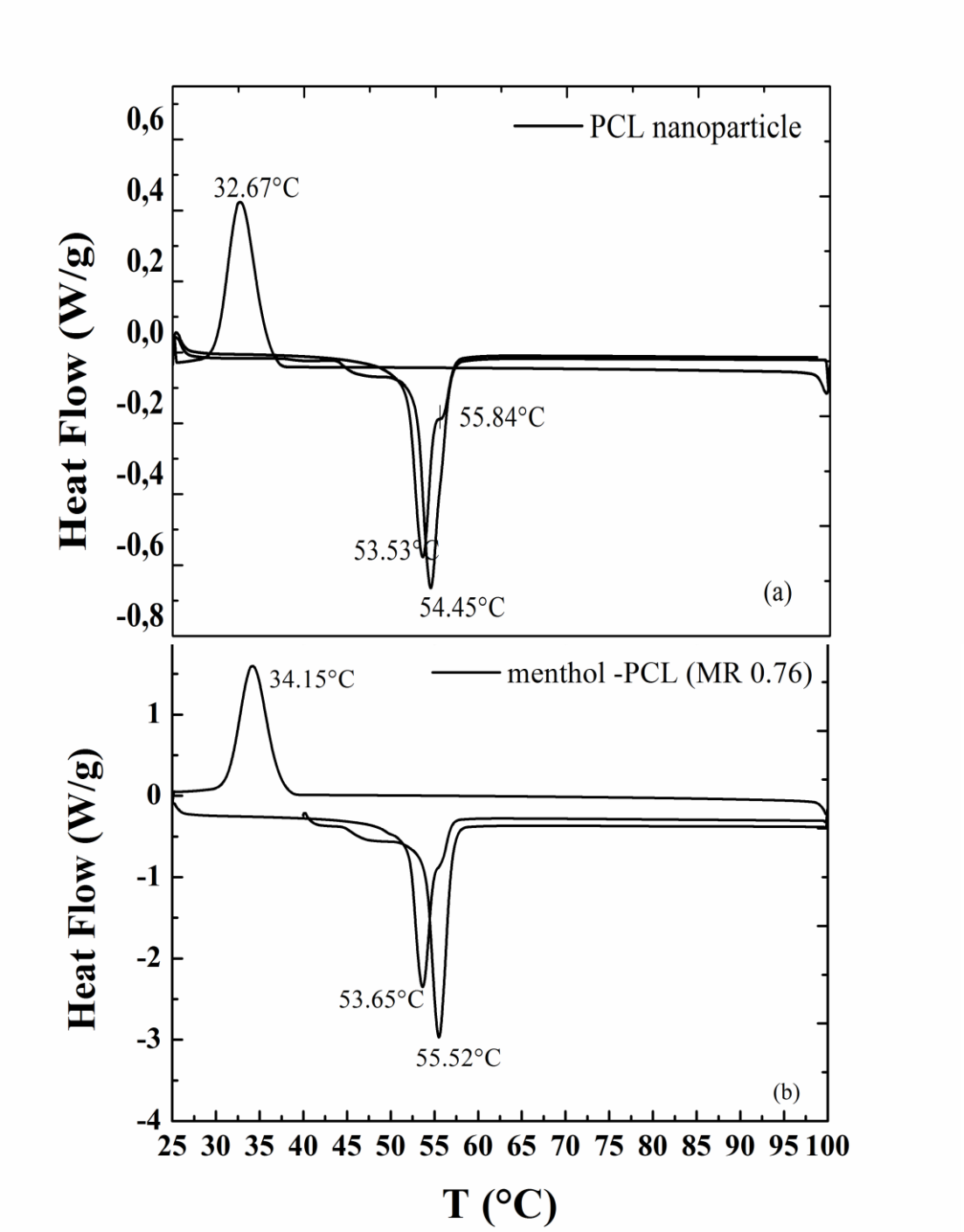

Figure S3. DSC thermograph: (a) PCL nanoparticles, C_{PCL} = 25 mg/mL; (b) menthol-loaded nanoparticles, C_{PCL} = 6 mg/mL, *MR*=0.76. Cyclic heating from 20°C to 100°C; heating and cooling rate: 5°C/min

Particle size distribution (PSD), Polydispersity index (PdI) and Zeta potential

The effect of solvent on menthol-loaded nanoparticle size was similar to that observed for unloaded PCL nanoparticles, namely the smallest particles were obtained with acetone, and larger with acetonitrile. Also the PdI varies in the same way for the different solvents. Some examples of the reconstitued PSD obtained with different quench ratios *QR* are shown in Figure S4 .

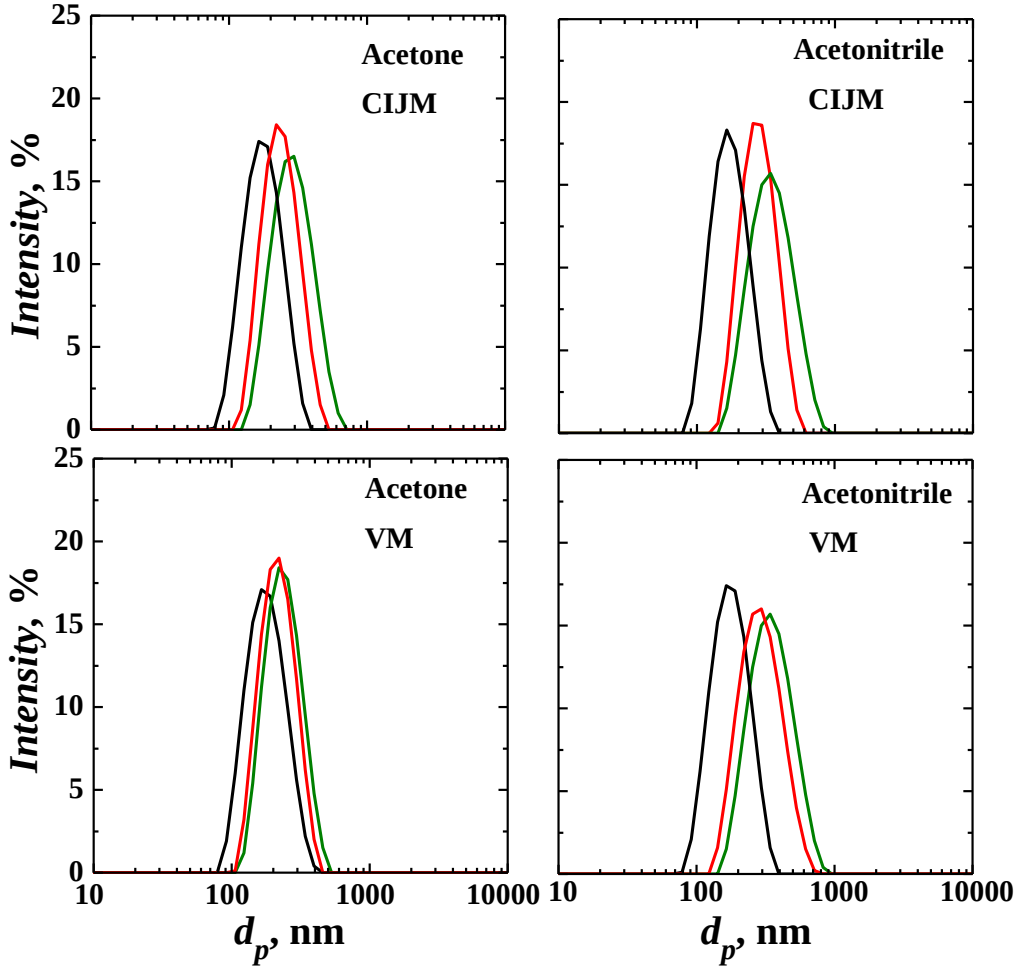

Figure S4. Particle size distribution (PSD) of menthol-loaded nanoparticles using acetone (left graphs) and acetonitrile (right graphs), in CIJM (upper graphs) and two-inlet VM (lower graphs). Quench ratio, *QR*: 0.12 black solid lines; 0.5 red solid lines; 1.0 green solid line. Inlet feed, C_{PCL}= 6 mg/mL, *MR*=0.76. Inlet feed velocity *Vj*=1.69 m/s (*FR*= 80 mL/ min).

An example of the particle size distribution obtained for loaded nanoparticles at different polymer concentration (and constant *MR*) is shown in Figure S5; it can be noted that increasing the PCL concentration the average sinze increases sligthly, but the dsitribution becomes broader.

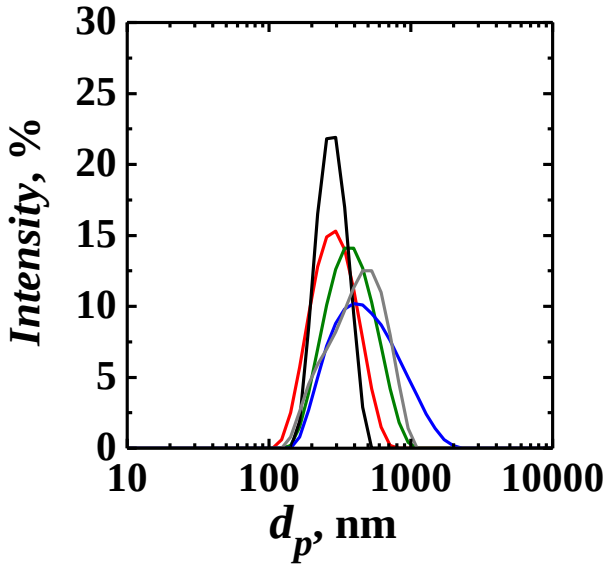

Figure S5. PSD of menthol-loaded nanoparticles produced in the CIJ mixer at different inlet stream velocity using acetonitrile, at menthol/PCL *MR*=0.76 and polymer concentration: $C_{PCL=}$ 3 mg/mL, black lines; 6 mg/mL, red lines; 9 mg/mL, green lines; 12 mg/mL, grey lines; 15 mg/mL, blue lines. Inlet feed velocity *Vj* =0.21 m/s. CIJM, *QR*=0.5.

This is confirmed by the analysis of the polydispersity index (see Figure S6) which shows that polydispersity is also significantly affected by the menthol/PCL ratio.

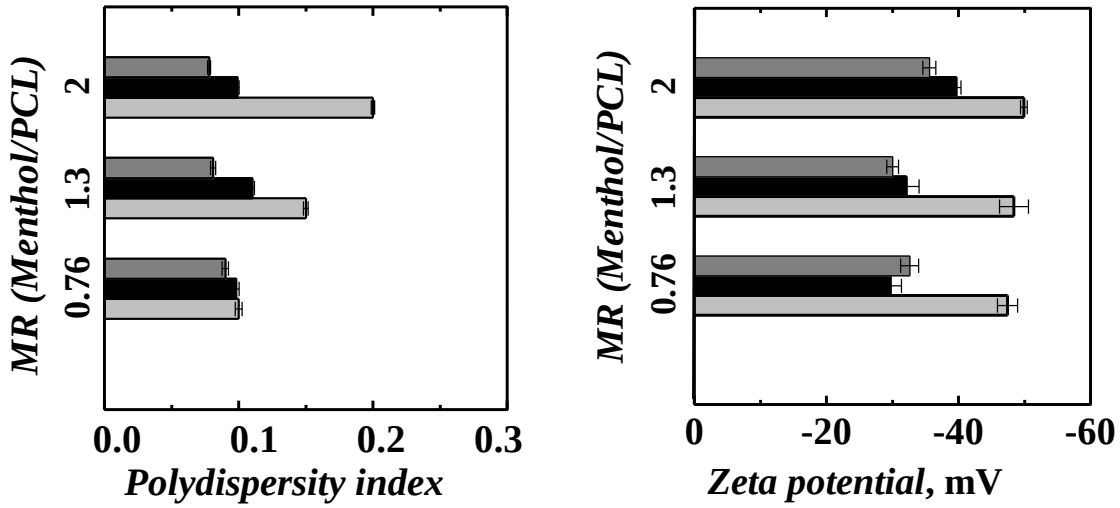

Figure S6. Polydispersity index (left) and Zeta potential (right) of menthol-PCL loaded nanoparticles in acetonitrile; a) *MR*=0.76; b) *MR*=1.3; c) *MR*=2.0. CIJM, *QR*=0.5. Inlet polymer concentration, C_{PCL}: 3 mg/mL, dark grey bars; 6 mg/mL, black bars; 9 mg/mL, light grey bars.
Inlet feed velocity *Vj* =0.21 m/s.

The effect of the different feeding configurations for the vortex type mixers is shown in Figure S7, that also shows the comparison for the two- and four-inlets vortex mixers, both for unloaded nanospheres and for menthol-loaded nanoparticles. The influence of the solvent in this mixer is the same previously reported for the CIJM, with systematically larger particles formed in acetonitrile.
The smallest particles were obtained in the SWWW (that is one solvent and three water streams) configuration; small differences are noted in the symmetrical and non-symmetrical configuration, with the water and solvent streams alternated (SWSW) or in sequence (SSWW) respectively.
As concerns the Zeta potential, the differences between the different configurations were small and, also for the vortex type mixers, values observed for loaded and unloaded particles were similar.

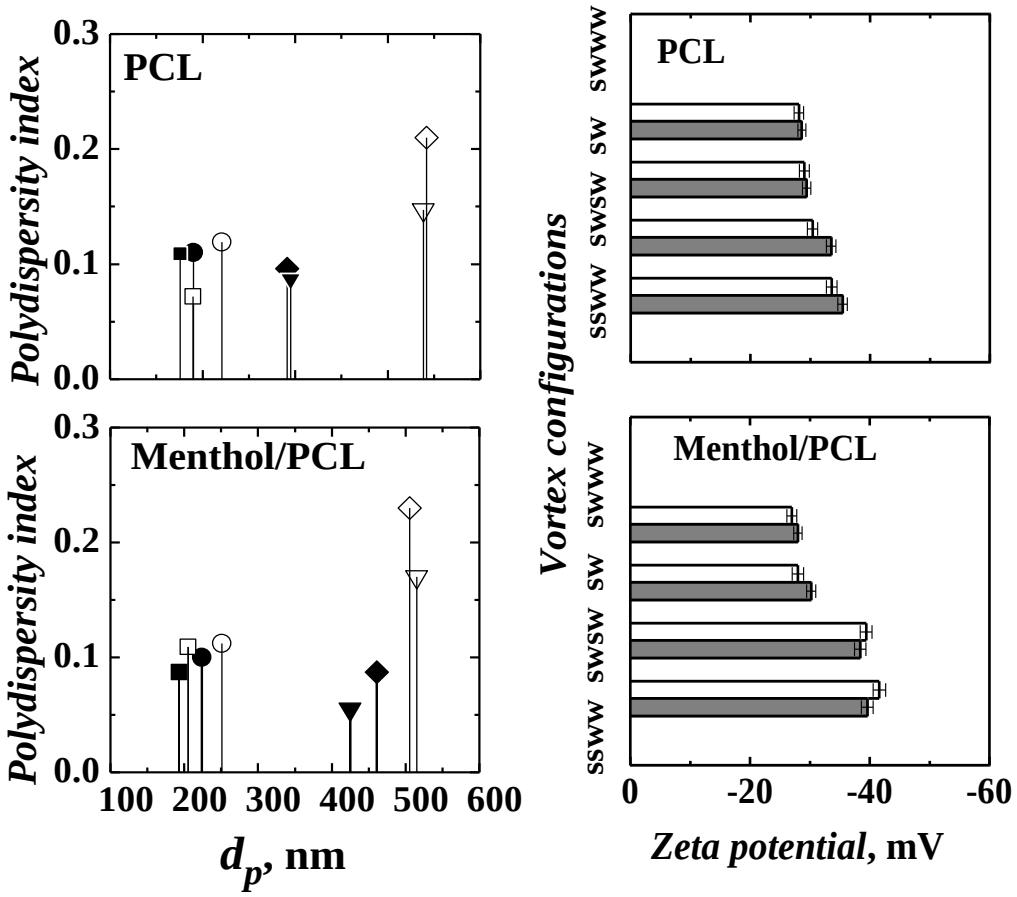

Figure A7. Polydispersity index (left graphs) and Zeta potential (right graphs) of the nanoparticles produced with acetone and acetonitrile, for PCL only nanospheres [PCL] and menthol-loaded nanoparticles [Menthol/PCL]. Left graphs: (a,b) Two-streams VM: ●,○. (*QR*=1). Four streams MIVM: ■,□, SWWW (no quench); ◆◇, SWSW (*QR*=1); ▼,▽, SSWW (*QR*=1). C_{PCL} =6 mg/mL, *MR*=0.76. Inlet feed velocity *Vj*=1.69 m/s. Right graph: (c,d) grey bars for acetone, white bars for acetonitrile. [Note that for the VM the data refer to a different experiment with respect to that shown in Figure 5h]